EMEP Report 1 and 2/2002
Date: July 2002

emep

Co-operative programme for monitoring and evaluation of the long range transmission of air pollutants in Europe

Transboundary acidification, eutrophication and ground level ozone in Europe

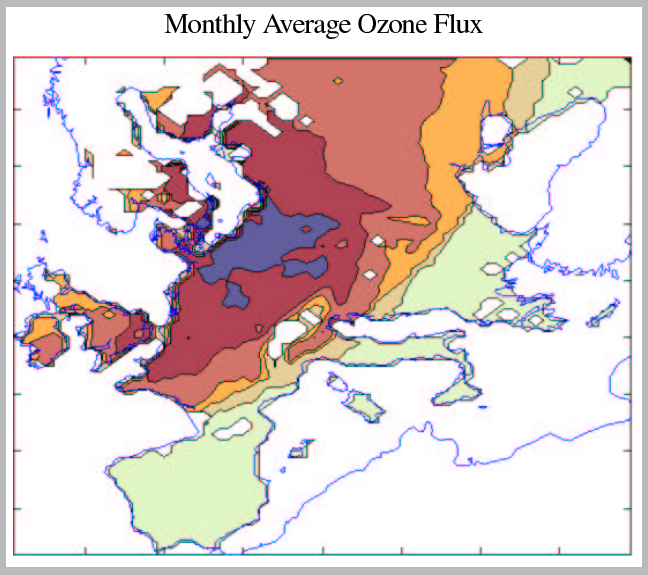

EMEP STATUS REPORT 2002

ccc & msc-w

EMEP Report 1&2/2002
Date: July 2002

METEOROLOGISK INSTITUTT
The Norwegian Meteorological Institute
Research Report No. 141

Transboundary Acidification, Eutrophication and Ground Level Ozone in Europe

EMEP Summary Report 2002

ISSN 0332-9879

Contributers

This EMEP MSC-W report has been produced as a result of collaborations between the scientists and institutions shown below.

Norwegian Meteorological Institute (MET.NO), Oslo, Norway

Anton Eliassen, Hilde Fagerli, Jan Eiof Jonson, David Simpson[a], Leonor Tarrasón, Svetlana Tsyro, Peter Wind and Åsmund Ukkelberg.

Centre for Ecology and Hydrology (CEH), Penicuik, Scotland

Ron Smith, Margaret MacDougall

Finnish Meteorological Institute (FMI), Helsinki, Finland

Juha-Pekka Tuovinen

Earth Science Centre (GVC), University of Gothenburg, Sweden

Yvonne Andersson-Sköld

Norwegian Institute for Air Research (NILU), Kjeller, Norway

Sverre Solberg

Stockholm Environment Institute at York (SEI-Y), University of York, England

Lisa Emberson

Dept. Environmental Science, University of Bradford, England

Mike Ashmore

(a) Also at GVC, Gothenburg, and Radio and Space Science, Chalmers, Gothenburg

Executive Summary

1. This report was prepared for presentation at the twenty-sixth session of the Steering Body to EMEP (Co-operative Programme for Monitoring and Evaluation of the Long Range Transmission of Air Pollutants in Europe). It provides an overview of modelling activities during 2001-2002, with an emphasis on the current state of the new unified EMEP modelling system.

2. This report is somewhat different in content to previous summary reports, in that we present the status of a model which is still undergoing change. No source-receptor calculations are presented. The latter is as agreed at the EMEP Steering Body and Executive Body, in the accepted workplan for EMEP for 2002.

3. The reason for this exceptional situation is that the EMEP MSC-W model has been undergoing a major overhaul, and efforts have been concentrated on the development, evaluation and improvement of the new model system. This overhaul was thought necessary in order to establish the best possible modelling system before policy-oriented modelling commences again as EMEP MSC-W's contribution to the UNECE Working groups and to the European Union's Clean Air for Europe (CAFE) initiative. It is planned to resume calculation of source-receptor matrices as soon as possible, and for presentation to the Steering Body of EMEP in 2003.

4. The previously separate photo-oxidant, acidification and aerosol models have been merged into one modelling system, denoted the Unified EMEP model system. Differences between the acidification (UNI-ACID), photo-oxidant (UNI-OZONE) and aerosol (UNI-AERO) versions of this model are now restricted to the necessary differences in chemistry and input treatment. Treatment of meteorology, emissions, transport and wet and dry deposition are now common to all versions.

5. This harmonisation work is almost complete. The model as it currently stands (July 2002) is believed to be comparable in performance to other Eulerian model systems.

6. The rv1.1 version of model has been evaluated by using an extensive set of measurement data. In addition model comparisons are shown with the preliminary rv1.2β version of the model.

7. Annual average of NO_2 concentrations for EMEP stations are in general within a factor of 2, and timeseries of NO_2 show the expected seasonal trends. Calculated concentrations of SO_2 and SO_4^{2-} correlate well with observations, both

in timeseries and as annual averages, but SO_2 is somewhat overestimated. Concentrations in precipitation of sum of nitrate, total sulphate and ammonia plus ammonium agree very well with observations, and for most stations the model data are within the '30% limit'.

8. Seasonal and daily variations in species such as ozone are reproduced well. The comparison with ozone-sonde observations show that the model overestimates ozone in the middle to upper free troposphere. The effect of this overestimation on surface ozone is likely to be limited. It is encouraging to see that for ozone and formaldehyde model results are improved with the rv1.2β version of the model.

9. A re-examination of the meteorological data on which the model is based has lead to a new focus on robust parameterisations, built around those data which are of known quality. Thus, we have now removed model parameterisations which depended on cloud liquid water because this parameter is not a verified output of meteorological models. Wet scavenging is now formulated in terms of precipitation, a parameter which does not allow such sophisticated physics, but which is routinely verified.

10. A similar focus on simplicity and robustness has lead to the use of climatological data for initial and boundary conditions for the models, instead of using data from global or hemispheric models.

11. Sensitivity analysis has demonstrated that the model's predictions of sulphur and nitrogen concentrations are only moderately sensitive to the formulations chosen for chemical parameters, at least within realistic bounds.

12. On the other hand, concentrations of all pollutants are very sensitive to the methodology chosen for vertical dispersion and mixing heights.

13. From these tests and other considerations, some areas of improvement have been identified, notably: evaluation of mixing height formulation, aqueous-phase oxidation scheme for SO_2, improved parameterisation of dry deposition for SO_2, NH_3 and other gases. These areas will be investigated and improved as appropriate.

14. As part of a Norwegian national project, the new model has been re-written to enable a flexible choice of the model resolution and the model domain. This will allow, among other things, to extend the EMEP model to describe intercontinental exchange of pollution in a hemispheric scale. It will also facilitate linking regional long range transport to urban and local scale pollution.

15. The work on nesting the EMEP model has just been initiated and it will take some time before this option becomes operative. In the meanwhile, much effort should be dedicated to re-write the model so that it is capable of operating with different meteorological input, in different scales (EMEP/MSC-W Note 5/2002).

16. The limitations of Eulerian models in providing source-receptor relationships have been evaluated. The results show that numerical errors associated with the representation of transport in Eulerian models are small when the physical extension of source regions to be analysed separately are sufficiently resolved. The conclusion

is that for European scale applications, the Eulerian EMEP model can provide country-to-grid source-allocation calculations with reasonable accuracy.

17. This conclusion is consistent with an independent quantification of numerical non-linearities in the EMEP model carried out for primary Particulate Matter. According to these calculations, numerical errors affect the calculation of source-receptor relationships for small European countries by introducing up to 10-15% differences between model runs and linear calculations. For most European countries, however, the numerical errors in the calculation of country-to-grid are below 3-5%. These results are reassuring for the capability of the Eulerian model to perform source-receptor calculations at European scale.

18. Further analysis on the effect of non-linearities associated with chemical and aerosol dynamics processes will be carried out as we engage into the calculation of source-receptor relationships with the Unified Eulerian model.

19. A preliminary model version is available which includes explicit calculation of stomatal fluxes for the first time. Calculations of ozone uptake have been made with the new model. The results, although preliminary, indicate that spatial patterns of stomatal uptake of ozone are rather different to patterns of AOT40. More work is needed on this model to include better land-use data and soil moisture effects.

Acknowledgements

The cooperations with the Finnish Meteorological Institute, Earth Sciences Centre (GVC, University of Gothenburg), Norwegian Institute for Air Research (NILU), Stockholm Environment Institute at York, England (SEIY), University of Bradford, England, Centre for Ecology and Hydrology (CEH, Edinburgh, Scotland) and the University of Oslo, Norway, are also gratefully acknowledged. Vigdis Vestreng and Anna Benedictow at met.no are thanked for providing the emissions and meteorological data-bases which make the modelling work possible. Heiko Klein is thanked for support with computing and graphics. Viel Odegaard and colleagues at the Norwegian Meteorological Institute are thanked for very valuable discussions on the meteorological data used in the EMEP models.

Work on the deposition module has also been financed by the UK Department of the Environment, Food and Rural Affairs (DEFRA), the Nordic Council of Ministers (NMR) and the Swedish Environmental Protection Agency (SNV).

The calculations presented in this report depend strongly on the meteorological data obtained from the Numerical Weather Prediction Model of the Norwegian Meteorological Institute. The calculations presented here have been made possible by access to the SGI and CRAY super-computers at the Norwegian University of Science and Technology (NTNU) in Trondheim, Norway.

Contents

Chapter 1

Introduction

1.1 Overview

This report presents a summary of the work conducted during 2001-2002 on acidification, eutrophication and photochemical oxidants within EMEP.

This report is somewhat different in content to previous summary reports, in that we present the status of a model which is still undergoing change. No source-receptor calculations are presented. The latter is as agreed at the EMEP Steering Body and Executive Body, in the accepted workplan for EMEP for 2002. The reason for this exceptional situation is that the EMEP MSC-W model has been undergoing a major overhaul, and efforts have been concentrated on the development, evaluation and improvement of the new model system. This overhaul was thought necessary in order to establish the best possible modelling system before policy-oriented modelling commences again as EMEP MSC-W's contribution to the UNECE Working groups and to the European Union's Clean Air for Europe (CAFE) initiative. It is planned to resume calculation of source-receptor matrices as soon as possible, and for presentation to the Steering Body of EMEP in 2003.

This report is organised in 8 chapters, mostly devoted to the unified EMEP model development and evaluation. Chapter 2 present an overview of the model and chapter 3 shows how the current model compares with measurements of a number of key species. Chapter 4 describes a number of sensitivity analysis, in order to illustrate how the model responds to reasonable changes in input parameters. In the course of model evaluation, it was found that there were problems in the physics and/or meteorology used to describe vertical mixing. The subsequent re-formulation of these processes is described in chapter 5. Chapter 6 describes work intended to probe the extent of non-linearity inherent in the use of a Eulerian model for source-receptor calculations. (chapter 8)

Finally, whilst chapter 7 does indeed discuss changes in the deposition scheme introduced to the latest version of the unified model, the main intent of this chapter is more applied. We present the first results of the stomatal flux modelling approach as applied in the full EMEP 3-D model. The results presented in this chapter suggest that stomatal-flux modelling is now a feasible proposition, and that mapping ozone damage based upon such an approach might give a very different spatial distribution to that suggested by AOT40 mapping.

It should be stressed that the unified modelling system is still undergoing changes, so no final version will be presented here. However, the model as currently coded is believed to be comparable to other Eulerian models and acceptable for both scientific and some policy-oriented studies. Indeed, the model has recently been used for two important applications: to provide boundary conditions for the CITY DELTA project under the EU DGXI Clean Air for Europe (CAFE) initiative[1], and as part of the EU DGXII project TROTREP[2].

A few improvements and evaluations are still planned before routine EMEP calculations re-commence. These include further evaluation of mixing height and vertical dispersion formulations, an aqueous-phase oxidation scheme for SO_2, and improved parameterisation of dry deposition for SO_2, NH_3 and other gases.

Descriptions of previous versions of the EMEP models, and their results, including source-receptor calculations, can be obtained from the EMEP web-site, http://www.emep.int. Details of the new unified model system will be added in the near future.

[1] By using a set of models on different scales CITY DELTA will assist air-quality managers in quantifying the contribution of regional versus local sources and in identifying and assessing the most effective emission control measures.

[2] Tropospheric Ozone and Precursors - Trends, Budgets and Policy. The prime objective of TROTREP is to evaluate, validate and predict the effectiveness of past and future EU air quality legislation with respect to ozone and its precursors

1.2 Other Publications

This summary report accompanies EMEP Report 5/2002 (EMEP, 2002), and EMEP MSC-W Note 4/2002 (Tsyro, 2002) which deal with the modelling and measurement activities of MSC-W and CCC on aerosols. A number of other reports and papers of relevance to oxidants and involving EMEP staff have become available in 2001/2002:

Peer-reviewed

- Emberson, L., Ashmore, M., Simpson, D., Tuovinen, J.-P., and Cambridge, H. Modelling and mapping ozone deposition in Europe. *Water, Air and Soil Pollution 130* (2001), 577–582.
- Johansson, M., Suutari, R., Bak, J., Lövblad, G., Posch, M., Simpson, D., Tuovinen, J.-P., and Tørseth, K. The importance of nitrogen oxides for the exceedance of critical thresholds in the Nordic countries. *Water, Air and Soil Pollution 130* (2001), 1739–1744.
- Simpson, D. *The EMEP MSC-W Lagrangian photo-oxidant model. Development, evaluation and applications*. Dr. philos. thesis, Faculty of Mathematics and Natural Sciences, University of Oslo, Norway, 2002.
- Simpson, D., Tuovinen, J.-P., Emberson, L., and Ashmore, M. Characteristics of an ozone deposition module. *Water, Air and Soil Pollution: Focus 1* (2001), 253–262.
- Tuovinen, J.-P., Simpson, D., Mikkelsen, T., Emberson, L., M., M. R. A., Aurela, Cambridge, H. M., Hovmand, M. F., Jensen, N. O., Laurila, T., Pilegaard, K., and Ro-Poulsen, H. Comparisons of measured and modelled ozone deposition to forests in Northern Europe. *Water, Air and Soil Pollution: Focus 1* (2001), 263–274.

Other

- EMEP, 2002, Transboundary particulate matter in Europe Norwegian Institute for Air Research, Kjeller, Norway, EMEP/MSC-W Report 5/2002.
- Tarrasón, L. and Jol, A. (eds.), 2002, 2000 PM emission data reported to UNECE/EMEP - Impact and evaluation of the CEPMEIP project, Norwegian Meteorological Institute, Oslo, Norway, EMEP/MSC-W Note 2/2002.
- Tarrasón, L., Kulmala, M. and Hansson, H.C. (eds.), 2002, Proceedings from NMR-UiHelsinki- EMEP "Workshop on implementation of aerosol dynamics in large scale applications", Norwegian Meteorological Institute, Oslo, Norway, EMEP Note 3/2002.
- Tsyro, S. 2002, First estimates of the effect of aerosol dynamics in the calculation of PM10 and PM2.5, Norwegian Meteorological Institute, Oslo, Norway, EMEP/MSC-W Note 4/2002.
- Vestreng, V. and Klein, H., 2002, Emission data reported to UNECE/EMEP: Emission total and sector trends & presentation of WebDaB, Norwegian Meteorological Institute, Oslo, Norway, EMEP/MSC-W Note 1/2002, June 2002.

1.3 References

EMEP, 2002, Transboundary particulate matter in Europe, Norwegian Institute for Air Research (NILU), Kjeller, Norway, EMEP Report 5/2002.

Tsyro, S. , 2002, First estimates of the effect of aerosol dynamics in the calculation of PM10 and PM2.5, MSC-W Note 4/2002.

Chapter 2

The Unified EMEP Modelling System

David Simpson, Hilde Fagerli, Jan Eiof Jonson, Svetlana Tsyro and Peter Wind

2.1 Introduction

The modelling tools previously available at EMEP MSC-W consisted of two main Eulerian models, the acidification model (MADE) of Berge (1998), Olendrzyński et al. (2000) and the oxidant model (MACHO) of Jonson et al. (1997,1998,2001). Additionally there were two Lagrangian models, one for acidification and one for photo-oxidants (Hov et al., 1988, Iversen, 1990, Simpson, 1993, Simpson, 1995). After years of separate development these models had codes which differed from each other in numerous ways, and even different physical descriptions of processes such as dry deposition and aqueous chemistry.

The new unified modelling system has been designed to provide a common core to all MSC-W modelling activities, building upon the Eulerian model structure. In the new system the only differences between say the acidification and oxidant versions lie in the chemical equations solved, and in the various inputs associated with this (for example, emissions and boundary conditions).

This chapter provides a brief overview of the model discussed in this report. As the work is ongoing, we will not present a detailed documentation of model equations. Rather, an overview is given, emphasising differences from previous model versions.

2.2 Revisions and Versions

There is of course a confusion in referring to different versions of a "unified" model. However, the unified EMEP model is a system rather than a single piece of code. The model version which is intended for full photochemical calculations obviously requires different chemical equations, emissions, and initial and boundary conditions, to a model intended only for looking at sulphur chemistry. By "unified" we mean that these differences between codes are minimised to that required for dealing with the different chemical schemes we are interested in.

Table 2.1: Recent Revisions and Versions of the Unified EMEP model

Revision	Version			Comments
	UNI-ACID	UNI-OZONE	UNI-AERO	
rv0.9			(s)	Early implementation, used for UNI-AERO development
rv1.0				Used for CITY DELTA project
rv1.1	(s)	(s)		Improved seasonal variation for dry deposition. Vertical exchange modified. Used for TROTREP Calculations
rv1.2β	(b)	(b)		Sub-grid deposition scheme, stomatal-flux calculation

Notes: (s) - last stable version; (b) - preliminary version available. For explanation of CITY DELTA, TROTREP see chapter 1.

We use the word "version" to distinguish between the different chemical systems we are dealing with. Thus, we typically use one version for acidification and eutrophication, with just 9 advected species, denoted UNI-ACID for convenience. For photochemical oxidants we use another version, UNI-OZONE, which has almost 70 reactive species and 140 reactions. Similarly, a preliminary UNI-AERO version has also been developed which is described in more detail in Tsyro (2002).

We use the word "revision" to denote the state of progress of the whole modelling system. The main differences between revisions have been mainly concerned with new treatments of dry and wet deposition, aqueous oxidation processes, treatment of boundary conditions, or vertical exchange processes. Thus, revision rv1.1 has improved dry deposition and vertical dispersion treatments compared to rv1.0. The latest revision is still under development, and is currently denoted rv1.2β. Ideally all versions of the model should be updated simultaneously, and this has indeed been the case for UNI-ACID and UNI-OZONE. The work on implementing dynamic aerosols in the EMEP model has been very time-consuming, however, and thus UNI-AERO is based upon a slightly older revision of the EMEP model than the ACID and OZONE versions. Table 2.1 summarises the latest revisions and places the different model versions in context.

2.3 Simplicity and Robustness

It should be noted that the unified Eulerian model has been simplified in several important respects when compared to the MADE/MACHO models from which it was derived. The main simplifications have been to:

1. Boundary conditions - default is now climatological
2. Oxidation of SO_2 to sulphate - simplified to avoid use of cloud liquid water (CLW)
3. Wet scavenging - simplified to avoid use of CLW.

The justification for all of these changes is basically the same: to construct the model around input data which we know is reliable or at the very least well characterised and stable.

For example, although model-derived boundary conditions provide some advantages in terms of 3-D coverage of many species, they suffer from the fact that no current model can reproduce observed concentrations of all species in a satisfactory manner for different seasons and locations. Typically, some species are simulated quite well, others rather poorly. Further, modelled boundary conditions have the disadvantage that 3-D fields are often inhomogeneous and thus difficult to visualise and interpret. With such fields it becomes very difficult to understand the contribution of the boundary conditions to particular chemical events occurring over Europe. Although observation-derived fields have disadvantages also, they provide a well-characterised input to the EMEP model and this eases the interpretation of atmospheric chemistry occurring in the model.

With regard to changes (2) and (3), the main justification for the change was the realisation that the cloud liquid water (CLW) which was provided by the NWP model was essentially of unknown validity. As a variable, CLW has little effect on NWP predictions and no routine data are available for verification purposes, so that little effort goes into establishing the accuracy of this parameter. Instead of using such a parameter in the EMEP model, we have now chosen to base the model's wet-scavenging on precipitation amounts alone, through the use of scavenging coefficients (section 2.4.9). Similarly, the aqueous phase oxidation of SO_2 to SO_4^{-2} is now calculated with the crude but well-characterised function given in section 2.4.6.

This example highlights a problem in air pollution which is often not clearly recognised, namely that not all of the meteorological data provided by Numerical Weather Prediction (NWP) models are reliable. Some parameters, such as pressure, temperature, wind and humidity, are thoroughly evaluated as part of normal weather forecasting and NWP model procedures. Other parameters, such as CLW and surface flux data, which are of great interest to air pollution modelling, are hardly evaluated at all, except during case-studies or field-campaigns. In future we will be placing a stronger emphasis on evaluation of the meteorological input data used by the model, and the constraints which uncertainties in such data place on the methodologies adopted.

2.4 Description of the Model

Here we give a brief overview of the unified model, with an emphasis on those aspects where the model differs from earlier Eulerian models.

2.4.1 Emissions

The treatment of emissions is largely unchanged from that used in previous photo-oxidant models. Emissions in 11 source categories (the so-called SNAP levels 1..11) are

input on the 50x50 km^2 grid as annual averages. These emissions are then distributed vertically according to a default distribution based upon the SNAP codes. Emissions are distributed temporally according to monthly (Jan.-Dec.), daily (Sun.-Sat.), and day-night factors derived from data provided by the University of Stuttgart (IER). Where required, biogenic emissions of isoprene are calculated hourly using the so-called E-94 system described in Simpson et al. (1995). Biogenic emissions of sulphur (DMS) are input as monthly average emission files, derived from Tarrasón et al. (1995).

2.4.2 Meteorology

The unified model uses 3-hourly resolution meteorological data from a dedicated version of the HIRLAM Numerical Weather Prediction model (Lenschow and Tsyro, 2000). This meteorology is identical to that used by the MADE model in recent EMEP reports. As noted in section 2.3 above, the evaluation of this meteorological data has been identified as one of the important themes of the model development and evaluation work at MSC-W.

2.4.3 Boundary Conditions

The boundary conditions system in the EMEP Unified model is very flexible. A pre-processing program interpolates the data field of interest (e.g. given in latitudinal/longitudinal grid squares) to the EMEP 150×150km^2 horizontal resolution and to the 20 vertical levels in the EMEP model. Currently, we use monthly averaged data fields, which are then read into the model once a month. However, the frequency of the update of the boundary conditions can be chosen freely, as long as the boundary condition field is provided for the same time period.

In the EMEP Unified model we distinguish between three types of boundary conditions:

- Initial conditions (IBC)
- Background conditions (BBC)
- Lateral + top of the model domain boundary conditions (LTBC)

We use IBC and LTBC for all relatively long-lived species, such as SO_2, O_3 etc. Background conditions are applied for species that are not explicitly included in the chemistry of interest, but that enter into reactions with some of the reacting chemical compounds. In UNI-ACID, we use background concentrations for O_3, OH, CH_3COO_2 (and H_2O_2, when aqueous chemistry of SO_2 is included). Only IBC and LTBC are applied in UNI-OZONE.

Ozone

Currently, two sets of monthly averaged O_3 background fields are available. The default set is derived from climatological O_3 data published by Logan (1998). Logan use sonde data in combination with surface and satellite data to derive gridded O_3 data of 4° latitude by 5° longitude for 13 pressure levels. A second set is available from the

University of Oslo, with values for 1997 calculated with the global model CTM2 (Sundet, Pers.comm). The model data has a resolution of 5.625°×5.625° with 19 vertical layers up to 10hPa. The two O_3 data sets are also used as IBC and LTBC.

Other Gases

In UNI-ACID concentrations of OH and CH_3COO_2 are prescribed by simple functions of the solar zenith angle. Values below clouds are reduced with a factor of 0.5 times the fractional cloud cover.

Concentrations of a number of other species are required. For example, UNI-OZONE uses CO, CH_3CHO, NO, NO_2, HNO_3, C_2H_6, C_4H_{10} and PAN, among others. These have been specified as simple functions, subjectively analysed to obtain values that correspond to observations (e.g., of Warneck, 1988, Solberg et al., 1996). The concentrations are adjusted in the vertical and for latitude and time of the year to match the observed distributions.

These distributions are preliminary, and alternatives derived at least partly from global CTMs exist. Further work is therefore required to evaluate the presently used boundary conditions.

2.4.4 Advection

Horizontal advection is based upon the scheme of Bott (1989a), Bott (1989b), as described in previous EMEP reports. However, some changes have recently been made in the advection algorithms, in order to allow flexibility in the choice of the grid resolution and meteorological data. This work will be described in detail in a forthcoming EMEP Note (EMEP Note 5/2002, in preparation), so only a brief outline is presented here.

Time Step Control

Numerical diffusion is one of the main limitations to the accuracy of the model. The size of the numerical diffusion will depend on the Courant number which in turn depend on the advection time step (Δt). In order to optimise the size of the time step, an automatic control of the time step has been implemented in the model.

Ideally we would like a constant Courant number equal to one, which will not result in any numerical diffusion. This is not feasible because the Courant number depends on the wind speed, which is varying in both time and space. If the grid resolution Δx is given, only the time step Δt can be adjusted. In earlier version of the model Δt was fixed at $\Delta t = 600$ s, which ensures that the Courant number remains less than one as long as the wind speed $|u|$ is less than 300 km/h (in the case $\Delta x = 50$ km). Usually wind speeds at the earth surface are much smaller. In addition to that, it is not unusual that the wind speed becomes larger than 300 km/h at high altitudes. In the new version the time step is determined dynamically during runtime. An exact formulation should also take into account the mapping factor m.

In a map obtained by projection, the gridwidth on the ground is usually not a constant. To take into account the variable size of each cell, the Courant number has to be multiplied by the mapping factor m:

$$c = m^2 \frac{\Delta t}{\Delta x}|u|(u = U/m)$$

If the wind speed u is positive on the right side of the cell ($u_j > 0$) and negative on the left side $u_{j-1} < 0$, the Courant criterion becomes:

$$c_{j-1} + c_j \leq 1(\text{when} u_{j-1} < 0 \text{and} u_j > 0)$$

The mapping factor is varying with j. The value of m in the upward cell has to be used. The explicit expression for the Courant criterion for a cell j can be written:

$$max(m_j^2 \frac{\Delta t}{\Delta x} u_j, 0) - min(m_j^2 \frac{\Delta t}{\Delta x} u_{j-1}, 0) \leq 1$$

Given values of m, Δx and u, a maximum value for Δt can be derived

$$\Delta t_{max} \leq \frac{\Delta x}{max(m_j^2 u_j, 0) - min(m_j^2 u_{j-1}, 0)}$$

For the vertical direction the corresponding expression in σ coordinates is:

$$\Delta t_{max}^{vert} \leq \frac{\Delta \sigma_j}{max(\dot{\sigma_j}, 0) - min(\dot{\sigma_{j-1}}, 0)}$$

The time step is put to the same value for all cells in each direction. For simplicity the time step in the two horizontal directions are also put to the same value.

The time steps in the horizontal directions can be different at different heights. The time step for the vertical advection can also be different from the time step in the horizontal directions.

After each advection call, the "time" in the different cells should of course be the same in the whole grid. The time between two advection calls is fixed (dt_advec) and the elementary time steps for the one dimensional advection have all to be an integer fraction of dt_advec.

dt_advec will control the time splitting error between the chemical and transport processes. Time-splitting errors can be reduced by reducing the time steps. A reduction of the time step will however increase the numerical diffusion errors. The time step must be determined as a compromise between these two requirements. The only way of reducing both time-splitting errors and the numerical diffusion is to increase the resolution of the grid.

2.4.5 Chemistry

Different chemical schemes are used for the UNI-ACID and UNI-OZONE versions of the model. The UNI-ACID scheme is based upon the simplified SOx-NOx-NHx chemistry as applied previously in the Lagrangian and Eulerian (MADE) acidification models

(Hov et al., 1988, Berge and Jakobsen, 1998). The UNI-OZONE scheme is based up the ozone chemistry from the Lagrangian photo-oxidant model (Simpson et al., 1993, Simpson, 1995), but with the addition of ammonium chemistry, taken from the UNI-ACID scheme. The formation of nitrate particles from HNO_3 in both models follows the procedure described by Jakobsen et al. (1997).

The implementation of chemical schemes in the unified model is now done using a pre-processor written in Perl. Thus, whilst the UNI-ACID and UNI-OZONE labels are convenient for describing two 'standard' chemistries within the modelling system, the new unified model can be quickly switched to accommodate new reactions and species.

As a relevant example, the unified model can also be run with the secondary organic aerosol formation scheme developed by Andersson-Sköld and Simpson (2001). This scheme was previously implemented in the Lagrangian oxidant model, but is now available for the 3-D model also.

The chemical equations are solved using the TWOSTEP algorithm tested by Verwer and Simpson (1995), using a fixed 60 s timestep. This scheme improves with iteration. In the 4 layers near the ground, where emission and often reaction tendencies are highest, we thus perform 3 iterations each timestep. Above this, 2 iterations are performed, except for the uppermost 6 layers where 1 iteration is believed sufficient.

2.4.6 Aqueous Chemistry

As noted in section 2.2, we have replaced the cloud-water-based aqueous oxidation of some species (notably $SO_2 \Rightarrow SO_4^{2-}$) with the very simple scheme similar to that used in early EMEP models (Hov et al., 1988, Berge and Jakobsen, 1998). The new scheme is simply:

$$SO_2 \Rightarrow SO_4^{2-} \qquad k = 3.0 \times 10^{-6} + 2.0 \times 10^{-6} \sin(2\pi(\text{day} - 80)/366)$$

Although less sophisticated than the previous schemes which explicitly modelled the role of H_2O_2 and O_3 in SO_2 oxidation, the simple formulation has proven successful in previous EMEP work, and doesn't require the specification of meteorological parameters which are very poorly defined. In future we hope to implement again a more scientific approach, as soon as the difficulties with input data are overcome.

2.4.7 Aerosols

In UNI-ACID and UNI-OZONE, aerosols consist of ammonium sulphate (actually, $(NH_4)_{1.5}SO_4$), ammonium nitrate and non-ammonium sulphate. A much more sophisticated scheme is available and has been implemented in the so-called UNI-AERO version of this model. Details are given in Tsyro (2002).

2.4.8 Dry Deposition

A resistance-based and sub-grid calculation of dry deposition for all gases has been implemented in the unified model revision rv1.2β as part of the work on stomatal flux modelling for ozone (see chapter 7). Although the ozone deposition rates contained

in this module have been evaluated rather well, further work is required in order to evaluate and improve the deposition of other gases, notably SO_2, NO_2 and NH_3.

Meanwhile, a simpler dry deposition scheme has been adopted for the model studies with rv1.0 and rv1.1. This scheme is derived from that used in the MACHO model and involves the specification of the 1 m deposition velocity (V_g) for each grid-square, based upon one of six land-use classes. Somewhat more complicated than MACHO, these V_g values have been specified as max (noontime) and min (nighttime) values, and adjusted for season and latitude in a similar manner to that of Hov et al. (1988). The drag-coefficient approach of Berge and Jakobsen (1998) is then used to estimate V_g values appropriate to the centre of the grid volume (ca. 45 m above ground level) and thus loss rates.

2.4.9 Wet Deposition

As noted in section 2.2, we have replaced the cloud-water-based deposition schemes used in the MADE and MACHO models with a simpler scheme based upon precipitation. Wet scavenging is now done using a simple scavenging coefficient, similar to the approach used in Berge and Jakobsen (1998).

2.5 References

Andersson-Sköld, Y. and Simpson, D. , 2001, Secondary organic aerosol formation in Northern Europe: a model study, *J. Geophys. Res.*, 106, No. D7, 7357–7374.

Berge, E. and Jakobsen, H. A. , 1998, A regional scale multi-layer model for the calculation of long-term transport and deposition of air pollution in Europe, *Tellus*, 50, 205–223.

Bott, A. , 1989a, A positive definite advection scheme obtained by non-linear renormalization of the advection fluxes, *Mon. Weather Rev.*, 117, 1006–1015.

Bott, A. , 1989b, Reply, *Mon. Weather Rev.*, 117, 2633–2636.

Hov, Ø. , Eliassen, A. , and Simpson, D. , 1988, Calculation of the distribution of NO_x compounds in Europe., In Isaksen, I.S.A. , editor, *Troposheric ozone. Regional and global scale interactions*, pages 239–262, Dordrecht. D. Reidel.

Iversen, T. , 1990, Calculations of long-range transported sulphur and nitrogen over Europe, *Science of the Total Environment*, 96, 87–99.

Jakobsen, H. A. , Jonson, J. E. , and Berge, E. , 1997, The multi-layer Eulerian model: Model description and evaluation of transboundary fluxes of sulphur and nitrogen for one year, EMEP/MSC-W Report 2/97, The Norwegian Meteorological Institute, Oslo, Norway.

Jonson, J.E. , Jakobsen, H.A. , and Berge, E. , 1997, Status of the development of the regional scale photo-chemical multi-layer Eulerian model, Norwegian Meteorological Institute, EMEP MSC-W Note 2/97.

Jonson, J. E. , Tarrasón, L , Sundet, J.K. , Berntsen, T. , and Unger, S. , 1998, The Eulerian 3-D oxidant model: Status and evaluation for summer 1996 results and case-studies, In *Transboundary photo-oxidant air pollution in Europe.* EMEP/MSC-W Status Report 2/98, The Norwegian Meteorological Institute, Oslo, Norway.

Jonson, J.E. , Sundet, J.K. , and L.Tarrasón, 2001, Model calculations of present and future levels of ozone and ozone precursors with a global and a regional model., *Atmospheric Environment*, 35, 525–537.

Lenschow, Hilde Sandnes and Tsyro, Svetlana , 2000, Meteorological input data for emep/msc-w air pollution models, EMEP MSC-W Note 2/2000.

Logan, J. A. , 1998, An analysis of ozonesonde data for the troposhere: Recommendations for testing 3-d models and development of a gridded climatology for troposheric ozone, *J. Geophys. Res.*, 10, No. D13, 16,115–16,149.

Olendrzyński, K. , Jonson, J.E. , Bartnicki, J. , Jakobsen, H.A. , and Berge, E. , 2000, EMEP Eulerian model for acid deposition over Europe, *Int. J. of Environmental Technology and Management*, in press.

Simpson, D. , Andersson-Sköld, Y. , and Jenkin, M. E. , 1993, Updating the chemical scheme for the EMEP MSC-W oxidant model : current status, Norwegian Meteorological Institute, EMEP MSC-W Note 2/93.

Simpson, D. , Guenther, A. , Hewitt, C.N. , and Steinbrecher, R. , 1995, Biogenic emissions in Europe 1. Estimates and uncertainties, *J. Geophys. Res.*, 100, No. D11, 22875–22890.

Simpson, D. , 1993, Photochemical model calculations over Europe for two extended summer periods: 1985 and 1989. Model results and comparisons with observations, *Atmospheric Environment*, 27A, No. 6, 921–943.

Simpson, D. , 1995, Biogenic emissions in Europe 2: Implications for ozone control strategies, *J. Geophys. Res.*, 100, No. D11, 22891–22906.

Solberg, S. , Dye, C. , Schmidbauer, N. , Herzog, A. , and Gehrig, R. , 1996, Carbonyls and nonmethane hydrocarbons at rural European sites from the Mediterranean to the Arctic, *J. Atmos. Chem.*, 25, 33–66.

Tarrasón, L. , Turner, S. , and Floisand, I. , 1995, Estimation of seasonal dimethyl sulphide fluxes over the North Atlantic Ocean and their contribution to European pollution levels. , *J. Geophys. Res.*, 100, 11623–11639.

Tsyro, S. , 2002, First estimates of the effect of aerosol dynamics in the calculation of PM10 and PM2.5, MSC-W Note 4/2002.

Verwer, J.G. and Simpson, D. , 1995, Explicit methods for stiff ODEs from atmospheric chemistry, *Applied Numerical Mathematics*, 18, 413–430.

Warneck, P. , 1988, *Chemistry of the Natural Atmosphere*, Academic Press, Inc., San Diego, California.

Chapter 3

Model Evaluation

Jan Eiof Jonson, Hilde Fagerli, David Simpson, Yvonne Anderson-Sköld and Åsmund Ukkelberg

3.1 Introduction

This chapter presents a large number of comparisons of modelled and observed concentrations and depositions, in order to illustrate both the state of the current stable version of the model (rv1.1) and of the model version which is under development (rv1.2β). Model calculations for the years 1995 - 2000 have been performed with the version rv1.1 of the UNI-OZONE model. In addition results from the UNI-ACID model are also presented. (The model versions are described in section 2.2, table 2.1). Although model calculations have been made for all the years 1995 - 2000, the focus is on years 1999 and 2000.

Note that, with the simplified oxidation scheme for SO_2, results for the sulphur species are identical for UNI-OZONE and UNI-ACID model versions. Depositions of other species are also very similar. Unless otherwise stated model results always refer to the UNI-OZONE model version rv1.1.

We start by presenting the data for other components than ozone as some of these species are useful in the understanding of the ozone chemistry (i.e. NO_2 is a precursor for ozone formation). In general these species have a residence time in the atmosphere ranging from a few hours to a few days. The natural variability even within the EMEP 50x50km grid is likely to be large, making such a model to measurement comparison a hard test for the model.

In the EMEP database the measurements are classified according to the quality of measurement data (Schaug et al., 2001). It should be noted that the quality classes do not account for the representability of the sites with respect to the surrounding area. For the scatter plots shown below only results of quality class C or better (within 30% uncertainty) are included. Furthermore for concentrations in air we require a 75% data coverage (273 days) in the measurements. In the scatter plots presented below the 50% limit and 30 % limits are defined so that the ratio between computed and measured satisfy the relation:

$$(1 - X) \cdot measured \leq \frac{computed}{measured} \leq \frac{1}{(1 - X) \cdot measured} \tag{3.1}$$

where X is 0.5 and 0.3, respectively.

3.2 Model Evaluation for the Nitrogen Components

Below, results are presented as scatter plots, and as time series for a few selected sites.

3.2.1 Scatterplots

Scatter plots have been made for all the years 1995 - 2000, but only results for year 1999 are depicted. Annual statistics for all the years are shown in Table 3.2.1 for NO_2 (also including results from UNI-ACID for the years 1999 and 2000).

Table 3.1: Tabulated mean measured and calculated concentrations for the same sites, for sites with quality classification A, and for sites with quality classification C or better. For the years 1999 and 2000 results from the UNI-ACID model version are presented in brackets. All concentrations are in μgm^{-3}. Also shown are correlations (corr.) between model and measurements and bias.

	Quality class A only				Quality class A, B and C			
Year	Obs.	Calc.	Bias	Corr.	Obs.	Calc.	Bias	Corr.
1995	1.07	1.19	11%	0.70	2.12	1.88	-10%	0.78
1996	1.01	1.35	34%	0.90	2.31	2.25	-2%	0.83
1997	1.10	1.38	25%	0.79	2.20	2.26	3%	0.78
1998	0.90	1.26	40%	0.81	2.16	2.23	3%	0.77
1999	0.80	1.20	50%	0.92	2.03	2.12	4%	0.77
1999*	(0.80)	(1.06)	(33%)	(0.93)	2.03	(1.86)	(-7%)	(0.73)
2000	0.81	1.18	46%	0.87	1.92	2.10	9%	0.81
2000*	(0.81)	(0.92)	(14%)	(0.86)	(1.92)	(1.79)	(-6%)	(0.83)

Notes: $*$ From UNI-AERO model.

In Figure 3.1 (left) measured and calculated NO_2 in air are compared for 1999. NO_2 is slightly overpredicted by the model. However, a few sites of quality class B or C are underpredicted by the model. Including only sites in quality class A leads to a marked overprediction by the model. As shown in Table 3.2.1 this pattern is repeated for all the years 1995 - 2000. NO_2 levels calculated by the UNI-ACID version of the model, with a simplified nitrogen chemistry, are consistently lower.

Concentrations of total nitrate in air (HNO_3 and ammonium nitrate) are overpredicted by the model (Figure 3.1 (right)). Whereas the dry deposition of HNO_3 in the gas phase is very rapid, the dry deposition of particulate nitrate (ammonium nitrate) is very slow. Thus, surface concentrations of total nitrate are very sensitive to the distribution between gas and particle phases.

3.2.2 Timeseries for NO_2

In Figure 3.3 time series for NO_2 are plotted for 4 stations. There is a tendency for the model to overpredict concentrations in winter, and to underpredict in summer. Correlations between model and measurements are mostly below 0.5. In particular in

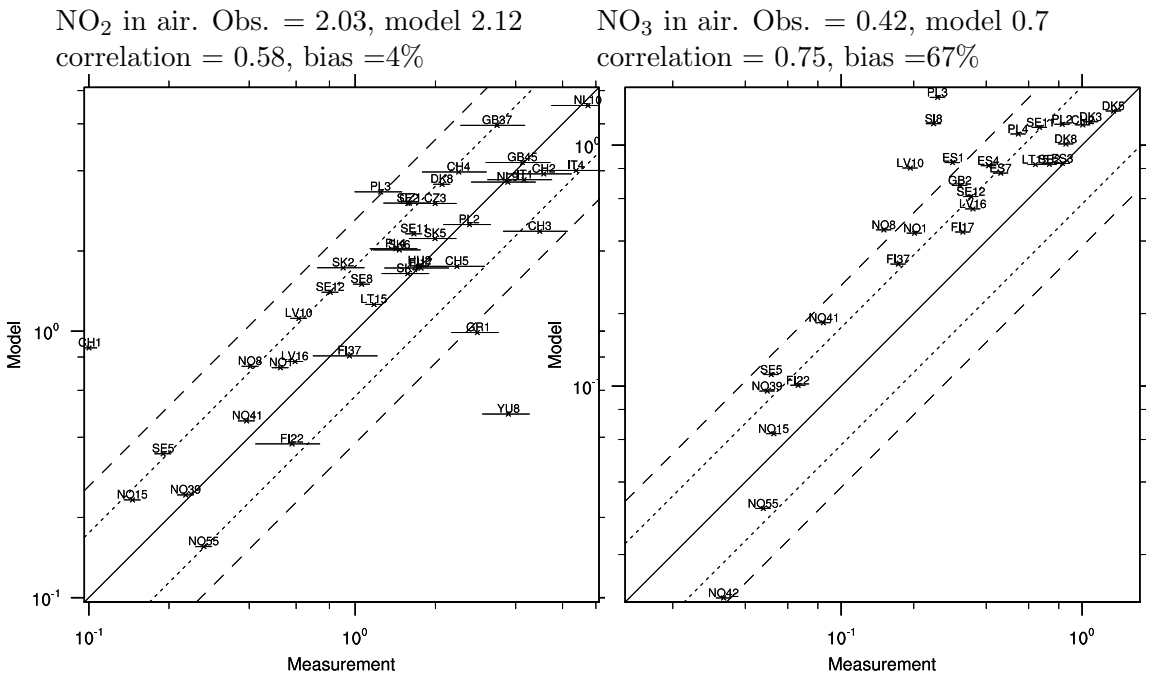

Figure 3.1: Scatter plots for measured and calculated annual mean concentrations of NO_2 in air (left), and HNO_3 (gas phase) and particulate nitrate (right). Concentrations in μg(N)m^{-3}.

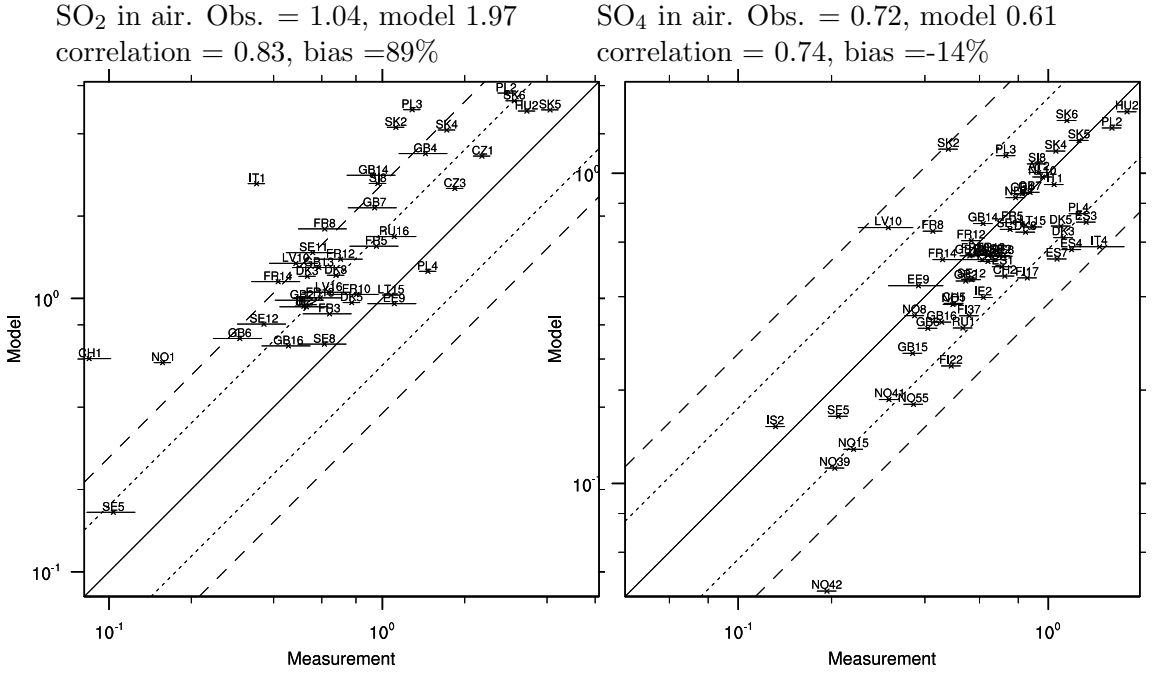

Figure 3.2: Modeled versus observed results for SO_2 and sulphate in air (μg(S)/m^3) for 1999: Annual average for all stations with expected data uncertainty (reported by CCC) $< 30\%$ and measurements for at least 75% of the days.

summer NO_2 has a chemical lifetime of hours only, and the variability within a 50x50km grid is large, making comparisons with point measurements difficult.

3.3 SO_2 and SO_4^{2-} in Air

The sulphur chemistry in UNI-OZONE and UNI-ACID is identical. As for the nitrogen species, model results for the sulphur species are compared to measurements both as scatter plots and as time series.

3.3.1 Scatterplots

In figure 3.2 the yearly average of SO_2 and SO_4^{2-} concentrations in air are presented. Modelled SO_4^{2-} concentrations are slightly underestimated (-14%) with respect to measurements, especially at the sites with the lowest concentrations. Correlations between measured and computed concentrations, calculated for annual means, are good both for SO_4^{2-} (0.74) and SO_2 (0.83). The calculated mean concentration for SO_2 is 89% higher than the the observations. Since the EMEP measurement stations are located in the background, far from local sources, the model grid square average should overestimate SO_2 concentrations. It is difficult to estimate how large this bias should be.

As noted in chapter 4, uncertainties in the dry deposition for SO_2 and in the very simple scheme for oxidation of SO_2 to SO_4^{2-} will lead to uncertainties in the calculated surface SO_2 concentrations. Further developments on these subjects should improve the results.

3.3.2 Timeseries for SO_2

In Figure 3.4 time series for SO_2 are plotted for 4 stations. As for NO_2, the model often overpredicts SO_2 concentrations in winter, but in contrast summertime SO_2 values can be either higher or lower than observed.

3.4 NH_3+NH_4^+ in Air

The chemical and physical properties of ammonia and ammonium are very different. Ammonia is a primary emission and efficiently dry deposited, thus a local pollutant, whereas secondary aerosol NH_4^+ is transported over long distances. Thus, for model evaluation, separate NH_3 and NH_4^+ measurements are desired. Unfortunately, very few independent measurements of gas and particle phases exist.

In Figure 3.5, the calculated (with UNI-ACID) yearly average concentration of ammonia plus ammonium are compared against measurements. The total ammonia plus ammonium concentration is overestimated by 36% in the model calculations. The correlation between measured and computed concentrations, calculated for annual means, is reasonable (0.66).

Ammonia plus ammonium concentrations calculated by UNI-ACID and UNI-OZONE are very similar. Ammonium sulphate concentrations are identical in the two versions, but HNO_3 is produced by slightly different pathways, thereby causing different interactions with ammonia. The resulting ammonia plus ammonium concentrations from

Birkenes, south Norway
obs = 0.52, mod = 0.73, corr. = 0.385

Preila, Lithuania
obs = 1.17, mod = 1.25, corr. = 0.422

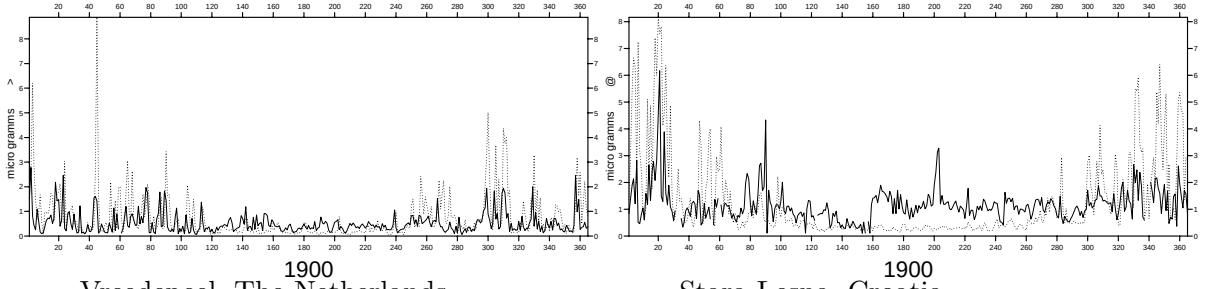

Vreedepeel, The Netherlands
obs = 7.45, mod = 7.00, corr. = 0.465

Stara Lesna, Croatia
obs = , mod = 49.64, corr. = 0.687

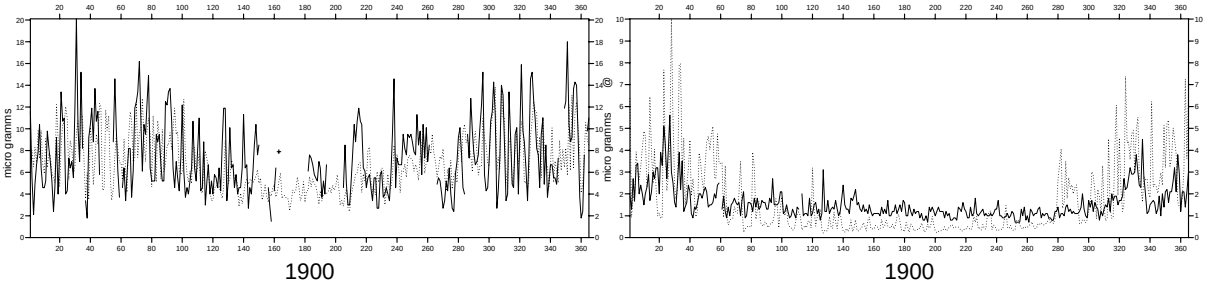

Figure 3.3: Measured (solid line) versus calculated (dotted line) daily mean concentrations of NO_2 in $\mu g(N)m^{-3}$ in 1999.

La Hague, France
obs = 0.95, mod = 1.55, corr. = 0.410

Preila, Lithuania
obs = 1.01, mod = 1.02, corr. = 0.728

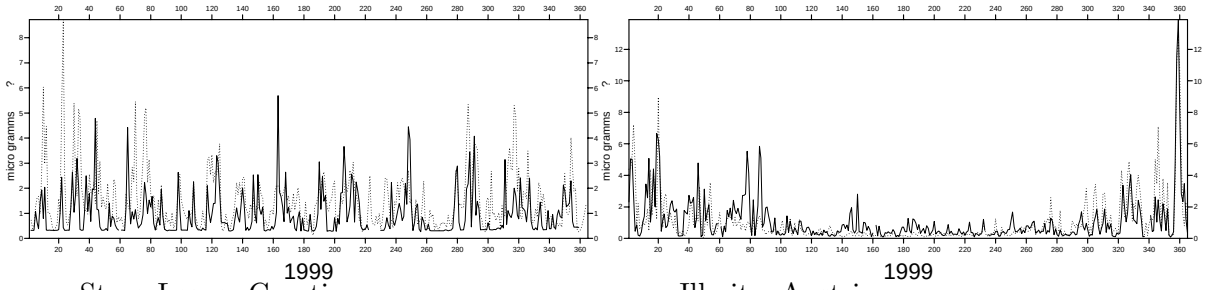

Stara Lesna, Croatia
obs = 1.72, mod = 4.11, corr. = 0.462

Illmitz, Austria
obs = 1.95, mod = 2.50, corr. = 0.589

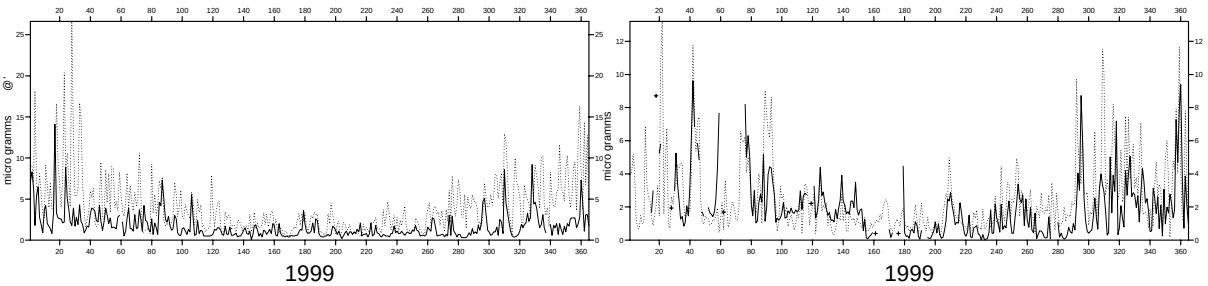

Figure 3.4: Measured (solid line) versus calculated (dotted line) daily mean concentrations of SO_2 in $\mu g(S)m^{-3}$ in 1999.

UNI-OZONE are in somewhat better agreement with observations (28% bias and 0.73 in annual correlation).

3.5 Concentrations in Precipitation

Figure 3.6 shows the differences between measured and computed total annual precipitation. It should be noted, however, that each model value refers to the grid cell mean, while the measured value refers to a point measurement. No point measurement can provide a good measure for an area equivalent to the grid cell area (ca. 2000 to 2500 km^2). Therefore, the relatively low annual correlation (0.62) between observations and modelled data is not surprising. The modelled precipitation mean (830 mm) is 14 % lower than observed (978 mm).

In figure 3.7 we present scatter plots for modelled (with UNI-ACID) versus observed concentrations in precipitation averaged over EMEP stations with quality better than C and at least 25 % common days of observation and model data. In general, the agreement between observations and model data is good. The scatter is small, and most stations are within the '30% limit'. The bias from measurements are within ± 10% both for total sulphate, total nitrate and the sum of ammonia and ammonium concentrations in precipitation.

Annual calculated means of wet deposition of sulphate, nitrate and ammonia plus ammonium (not shown) are underestimated by 17%, 36% and 28%, respectively, compared to observations. This can partially be explained by the underestimation of precipitation at most stations. Results from UNI-ACID and UNI-OZONE are very similar for the components discussed in this section and we have therefore chosen to show only the results from the UNI-ACID model version.

3.6 Aldehydes

Version rv1.1 and rv1.2β of UNI-OZONE have been compared with EMEP measurements of aldehydes. As aldehydes are strongly linked to the photochemistry in the nearest hours and days prior to the measurements, they are potentially well suited for validation of the model's photochemical parameterisation, and previous comparisons have indicated a very good agreement between model calculations and observations. For the 2000 data there are several points to keep in mind regarding the carbonyl measurements when comparing with the model predictions.

UBA started carbonyl measurements at three new German sites in 2000, Zingst, Schmucke and Brotjacklriegel (not included in this comparison) and also did the chemical analyses at their own lab including the analyses for Waldhof. Results from parallel measurements between NILU and UBA at Waldhof indicate an overall good agreement between the two laboratories' data although UBA's values are systematically higher. Furthermore, the results indicate that the agreement between the time series improved during the year. Whereas a marked bias is evident during February-May, the bias is clearly reduced after May. UBA started their carbonyl measurements in the last months of 1999 and was still in a learning and development phase by the beginning of 2000.

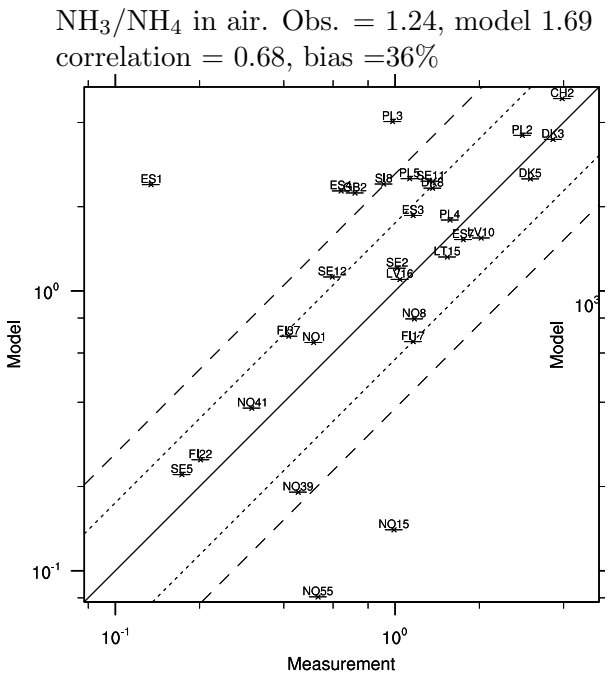

Figure 3.5: Modelled (UNI-ACID) versus observed results for NH_3+NH_4^+ in air (μg(N)/m^3) for 1999.

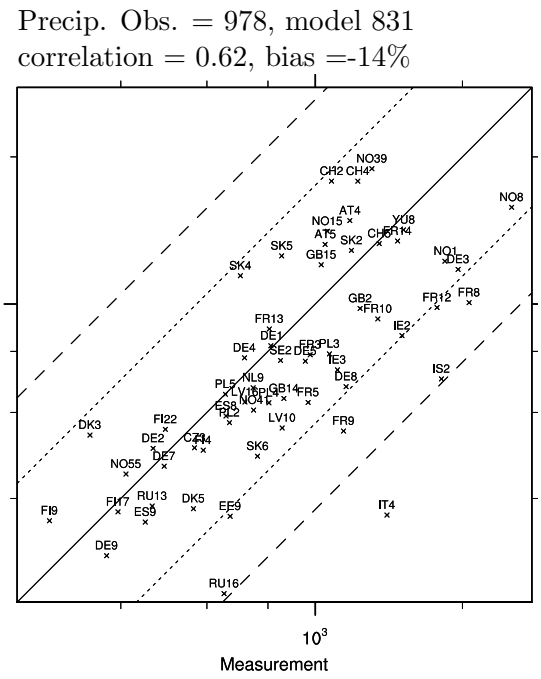

Figure 3.6: Computed versus measured annual average for all stations with measurements for at least 25% of the days.

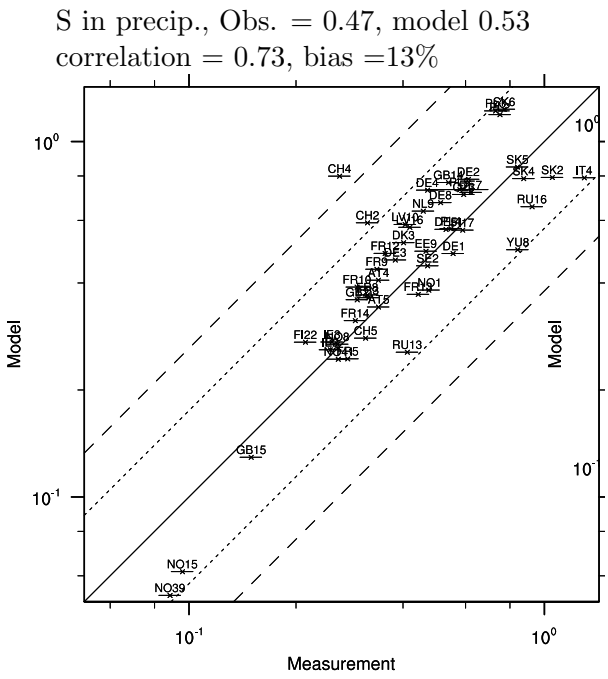

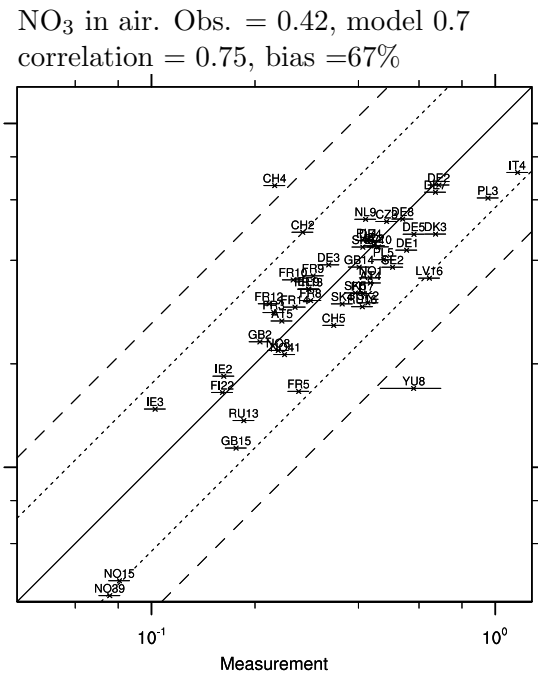

Figure 3.7: Modelled versus observed results for sulphate (left) and total nitrate (right) concentrations in precipitation (μg(N)/l) for 1999: Annual average for all stations with expected data uncertainty (reported by CCC) $< 30\%$ and measurements for at least 25% of the days.

In Figure 3.8 formaldehyde calculated with rv1.1 and rv1.2β of the UNI-OZONE model are compared to measurements. For all virtually all sites the rv1.2β version is in better agreement with measurements. The dry deposition of these species was not included in version rv1.1. This should explain most of the differences between the two model versions.

3.7 Model Evaluation for Ozone

Calculated ozone is compared to both surface measurements and for vertical profiles. For surface ozone some results with the rv1.2β version are also shown.

3.7.1 Surface Ozone

In Figure 3.9 measured and calculated daily maximum ozone are depicted for selected sites in different European regions in 1999. Such plots are also made for the years 1995 - 1998 and results for these are similar in terms of model performance and are therefore not shown.

The model performance is in general good. Major ozone events are reproduced by the model, resulting in high correlations between model and measurements at most sites. However, at many sites there is a tendency for the model to underpredict winter ozone and also spring ozone at high latitudes. Part of this may be explained by an overprediction of NO_2 in winter as discussed in section 3.2. However, it is interesting to see that with the new dry deposition scheme described in chapter 7 model calculated surface ozone are often improved compared to measurements (Figure 3.10). In particular for the site Esrange, where the rv1.1 performs poorly in winter and spring, model results are significantly improved.

3.7.2 Vertical Ozone Profiles

Sonde measurements of ozone are made at a number of sites in Europe. Ozone sonde data are archived at NILU as part of the project THESEO (Third European Stratospheric Experiment on Ozone - Ozone loss in the Arctic and at Mid-latitudes). The frequency at which measurements are made varies greatly from site to site. For several sites sondes are only released in winter or very infrequently in other parts of the year, reflecting the interest in stratospheric ozone depletion in the winter and early spring months.

From the middle troposphere and to the top of the model domain (100hPa) ozone levels are to a large extend determined by the lateral boundary concentrations as the chemical lifetime is long (of the order of one month) and horizontal advection is very fast compared to the vertical exchange. Thus, the model comparison with sonde data serves more as a test for the quality of the lateral boundary concentrations than internal model chemistry.

There is a tendency for the model to underpredict ozone levels in the stratosphere. As the vertical exchange across the tropopause is very slow this will have virtually no effect on concentrations in the troposphere. It is encouraging that concentrations in the lower/middle troposphere are mostly well reproduced with the exception of Valencia, where concentrations are underpredicted (at least in winter). In the lower

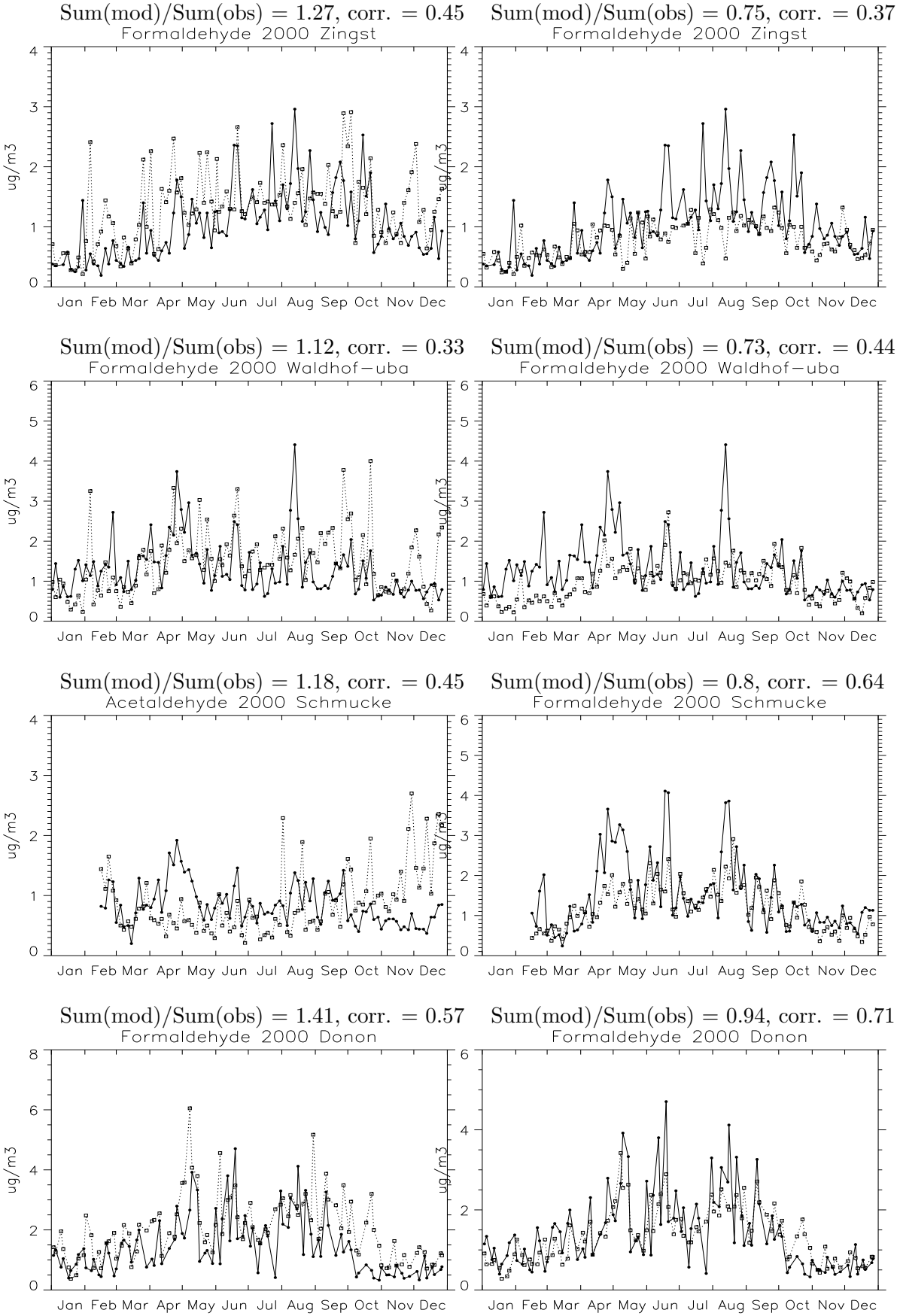

Figure 3.8: Measured model calculated formaldehyde in μgm^{-3} averaged between the hours 8 and 16 UTC in 2000. Left, calculated with rv1.1 and right with rv1.2β. Measurements (full line), model (dotted line).

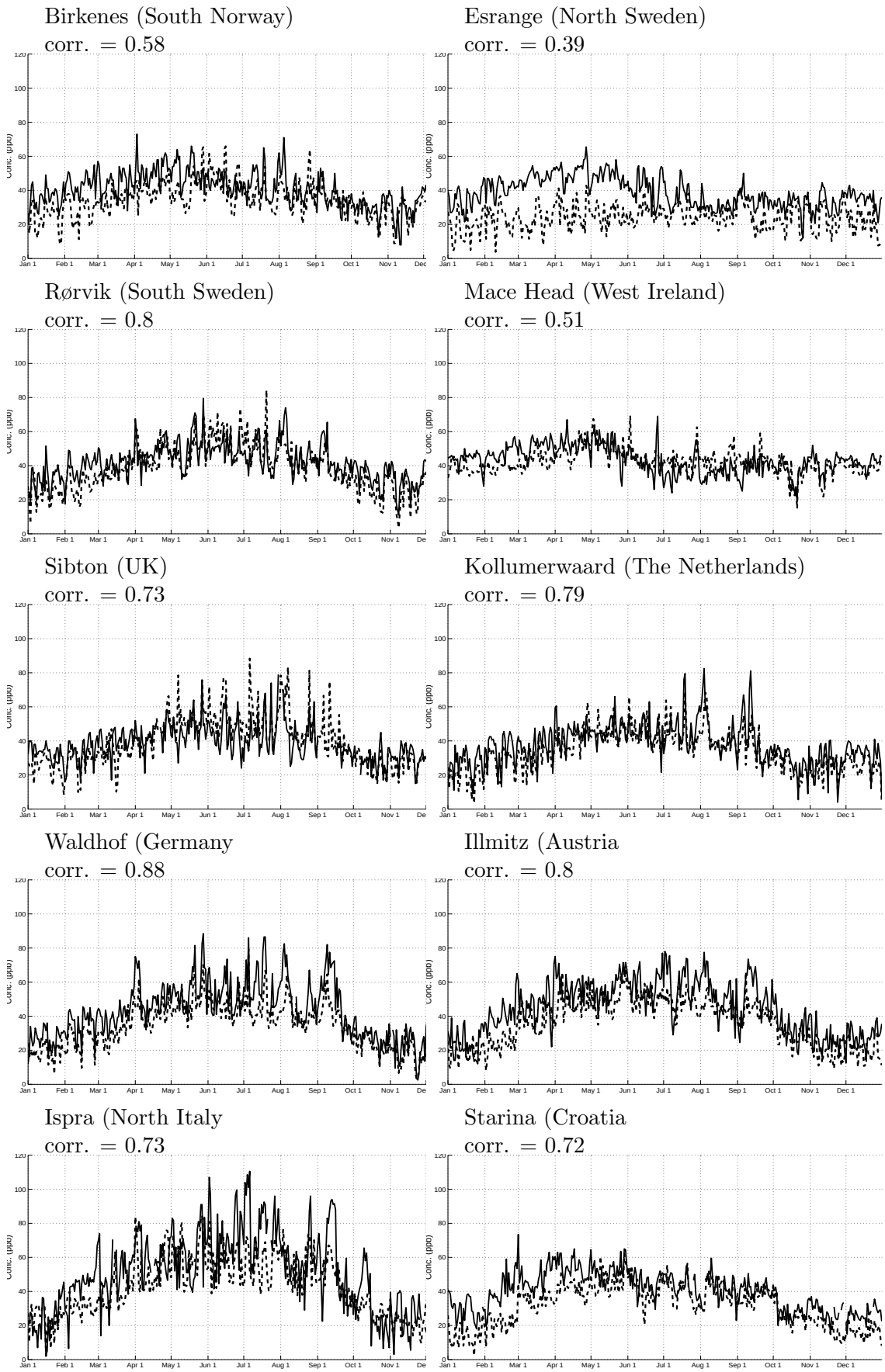

Figure 3.9: Measured versus calculated daily maximum concentrations of ozone in ppbv in 1999 with the rv1.1 model version of UNI-OZONE.

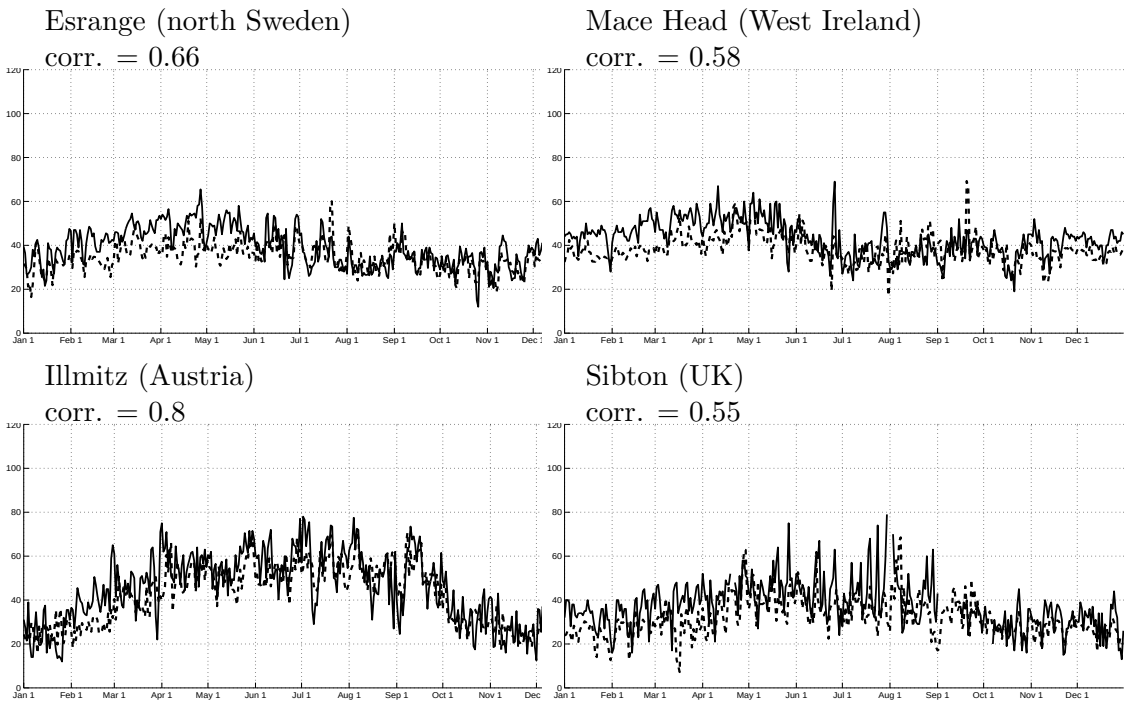

Figure 3.10: Measured versus calculated daily maximum concentrations of ozone in ppbv in 1999 with the rv1.2β model version of UNI-OZONE.

free troposphere the influence of boundary layer chemistry should be substantial. In the upper/middle troposphere concentrations are often overpredicted. As for the free troposphere ozone levels here are to a large extent determined by the lateral boundary concentrations.

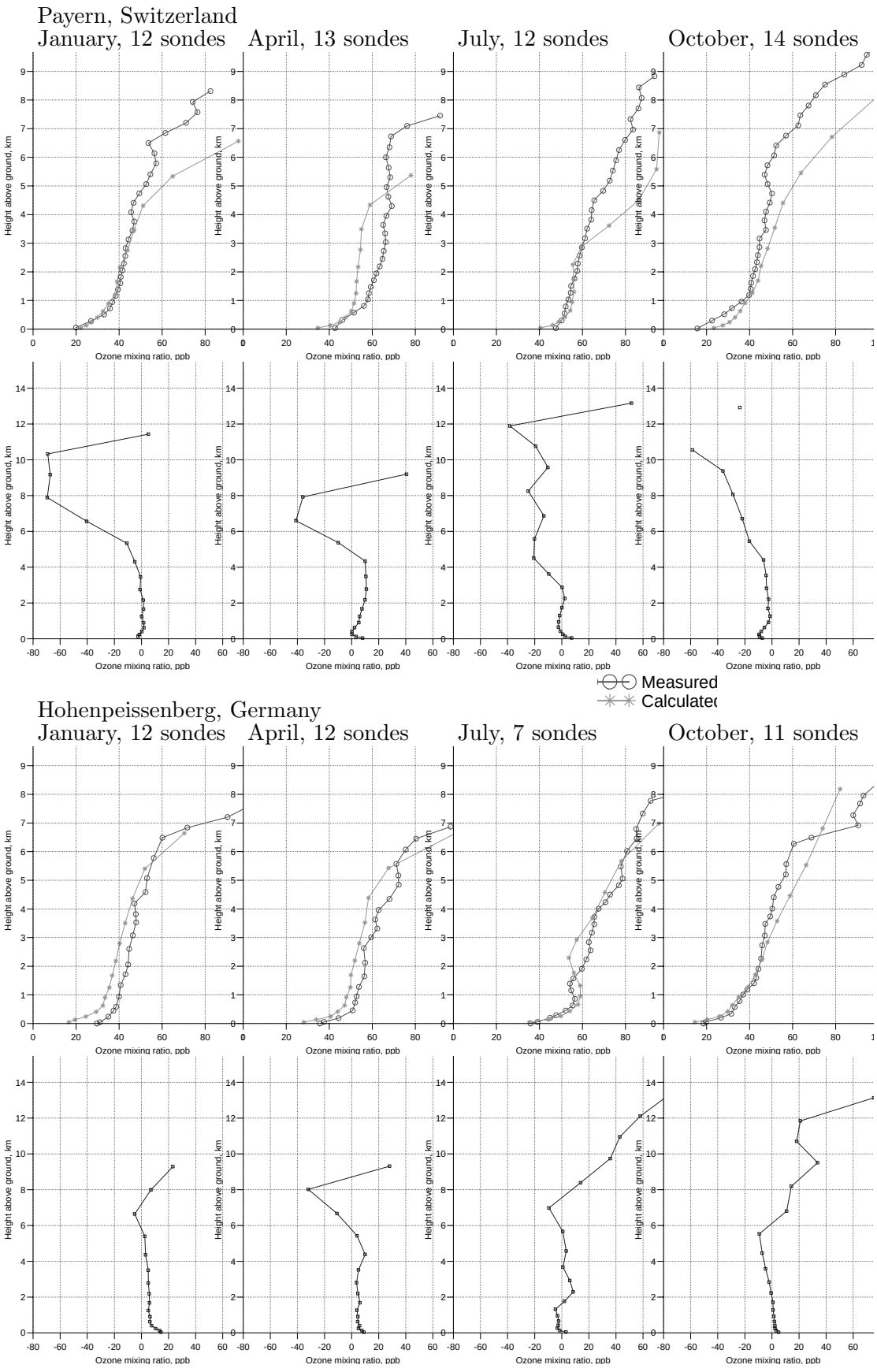

Figure 3.11: Ozone sonde measurements and model calculated ozone at Payerne and Hohenpeissenberg in 1999. Average of all sonde releases in January, April, July and October. Plots with single line depicts the difference between measurements and model (measured-calc.) for the figure above.

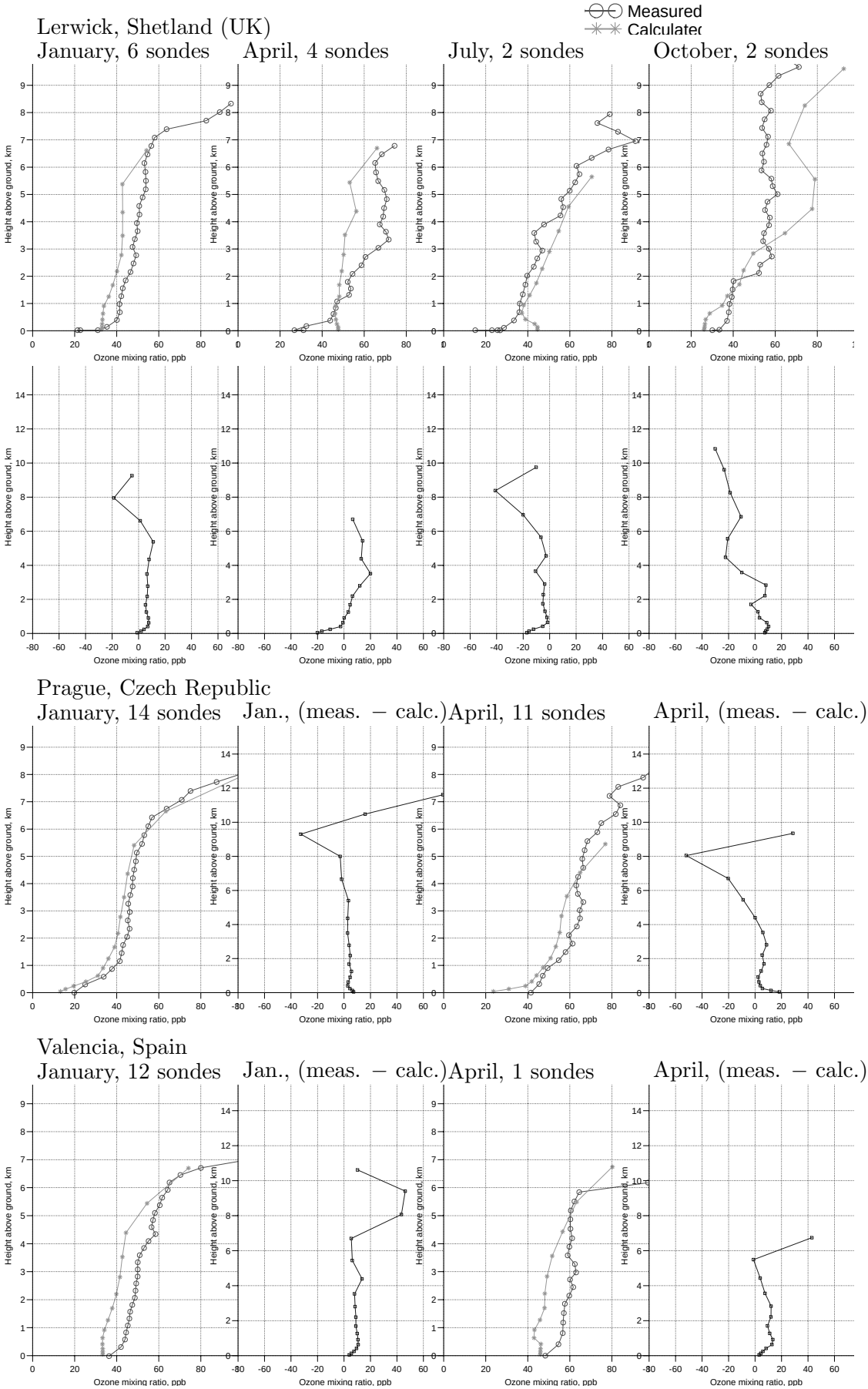

Figure 3.12: Ozone sonde measurements and model calculated ozone at Lerwick, Prague and Valencia in 1999. Average of all sonde releases in January, April, July and October (last 2 months only Lerwick). For Lerwick plots with single line depicts the difference between measurements and model (measured-calc.) for the figure above. For Prague and Valencia differences are shown alongside.

3.7.3 Diurnal Variations in Ozone

The diurnal variation of ozone at the surface represents the effects of both chemistry and deposition. Daytime values are somewhat elevated as a result of photochemical activity. Nighttime values are often reduced as a result of dry deposition to the surface and titration with available NO (e.g. from local traffic sources). These latter effects are most pronounced near the surface, because of the low vertical dispersion rates occurring in stable nighttime boundary layers. Ozone levels at higher levels are much less affected by nocturnal losses (e.g. PORG, 1993).

Figure 3.13 illustrates how well the model (rv1.2β) captures the diurnal variation of two UK sites. As well as the model's predictions of surface ozone, we also illustrate the model's predictions of ozone at upper levels. The strong diurnal variation at Harwell and the weaker one at Bush are both reproduced in the surface concentrations. At higher levels ozone concentrations at both locations are seen to show almost no diurnal variation whatsoever, consistent with observations made at mountain sites in the UK (e.g. PORG, 1993). It should be admitted that not all sites show such good results. Coastal sites in particular seem difficult to capture, and we suspect that this is due to difficulties in specifying the correct stability regime for these grid squares. Work will continue to understand these diurnal cycles at different sites.

3.8 Summary

The rv1.1 revision of the UNI-OZONE and UNI-ACID models has been evaluated by using an extensive set of measurement data. In addition model comparisons are made with the preliminary rv1.2β version of the UNI-OZONE model. For most species the model compares favourable with measurements. Although there are differences in model validation between the UNI-OZONE and the UNI-ACID model, their results, in particular for wet removal are now very similar. SO_2 and total nitrate are overestimated by the model. The oxidation of SO_2 and the distribution between HNO_3 (gas phase) and particulate nitrate will be studied further. The comparison with ozone-sonde observations show that the model overestimates ozone in the middle to upper free troposphere. The effect of this overestimation on surface ozone is likely to be limited. It is encouraging to see that for ozone and formaldehyde model results are improved with the rv1.2β version of the model.

3.9 References

PORG, 1993, *Ozone in the United Kingdom 1993*, UK Dept. of the Environment, London, UK, Third Report of the United Kingdom Photochemical Oxidants Review Group.

Schaug, J. , Solberg, S. , and Aas, W. , 2001, EMEP measurement data quality, In *Transboundary acidification, eutrophication and ground level ozone in Europe* Status Report 1/2001, CCC&ciam&msc-w.

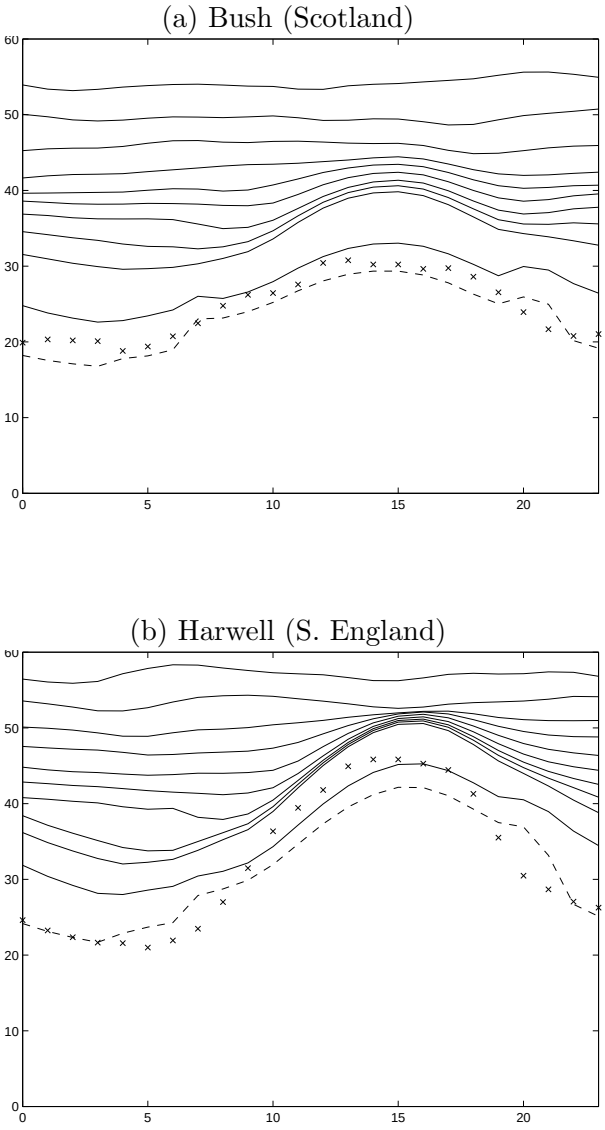

Figure 3.13: Observed (crosses) and Calculated Ozone (ppb) at two UK Sites. The dashed line shows the modelled O_3 at 1-m above the surface. The modelled O_3 concentrations for the lowest 10 levels of the model (solid lines) are also shown. The lowest level corresponds to about 45 m, the highest shown here to about 1700 m

Chapter 4

Sensitivity Tests

Hilde Fagerli

In order to understand why a model performs well or not, it is important to understand how sensitive the model is to changes in its input parameters or formulations. This chapter discuss the results of some sensitivity tests performed with the EMEP Unified model. The UNI-ACID version is used since this is the least computer-intensive version and anyway contains the same sulphur chemistry as the UNI-OZONE version. We investigate the sensitivity of SO_2 to the choice of deposition value, to the release height of the SO_2 emissions and to the SO_2 oxidation rate. In addition, we study the effect of different background values of O_3 and OH on surface concentrations of NO_2. Finally, the influence of the NH_4^+ to SO_4^{2-} ratio in $(NH_4)_x(SO_4)_y$ on air concentrations of ammonia+ammonium and nitrate in air is investigated.

4.1 Sensitivity Tests for SO_2 and SO_4^{2-}

4.1.1 SO_2 Deposition Value

The dry deposition process of SO_2 is complex and depends both on the land cover and the meteorological conditions. In addition, the presence of surface water on leaf surfaces and the chemical composition of the surface water can have a marked effect on the dry deposition. It has been shown that the ratio of NH_4^+ to SO_4^{2-} at wet surfaces is of large importance in this respect (Fowler et al., 2001). Since SO_2 emissions in Europe have decreased substantially over the last twenty years, whereas NH_3 emissions have changed relatively little, the NH_4^+ /SO_4^{2-} may be expected to have changed substantially, thereby increasing the dry deposition velocity.

In the EMEP Unified model (version rv1.1) we currently have a simplified scheme for dry deposition, where each specie is assigned a max (noontime) and min (nigh time) deposition velocity at 1 meter (V_g), appropriate to each land-use category. At night the deposition velocity, V_g, is simply set to V_g^{min}. During daytime an average deposition rate is approximated by V_g^{min} + 0.8 (V_g^{max}-V_g^{min}). For SO_2, the min/max values of the dry deposition velocity have been set to $V_g = 0.3/1.0$ cm s^{-1}, respectively. The loss rate is further adjusted for latitude, and time of the year, so that in general the loss rate is somewhat lower than given by V_g directly. The effective dry deposition velocity in the lowest model layer is found by modifying V_g with the calculated aerodynamic resistance over the surface layer (assuming the mid point of the lowest model layer to be the top of the surface boundary layer).

The procedure used to calculate variations in deposition velocities over the surface layer is also used to calculated a vertical gradient in concentrations. In well mixed conditions, the concentration of SO_2 at the surface is similar to the concentration in the lowest model layer. In more stable conditions, the concentrations at the surface can be significantly lower that the concentrations in the lowest model layer. The magnitude of the correction based upon this surface layer parametrisation depends on the deposition velocity: a higher deposition velocity leads to a greater gradient and thus a lower surface concentration.

For the preliminary rv1.2 revision of the EMEP model, a resistance approach has been used for all gases (chapter 7). However, the resistance analogy dry deposition scheme is complex and depends on many variables which are not well known (e.g. LAI, surface wetness). In addition, none of these deposition schemes take into account co-deposition of NH_3 and SO_2 which can be important (Fowler et al., 2001). It is clear that there are large uncertainties in any model of SO_2 deposition, and that this will lead to uncertainties in the calculated SO_2 surface concentrations.

As a sensitivity test, the SO_2 dry deposition velocity was increased by 50%. Table 4.1 shows model results for 1999, averaged over all EMEP stations with quality better than ±30%. Scatter plots for SO_2 and SO_4^{2-} are given in figures 4.1 and 4.3. The SO_2 concentration decrease by 20% in the calculation with the higher V_g. The results show that a precise prediction of SO_2 dry deposition velocities is important in order to calculate accurate surface concentrations of SO_2.

4.1.2 SO_2 Oxidation Rate

In the gas phase, the reaction with OH is the dominant path oxidising SO_2 to sulphate. However, the bulk of the production of SO_4^{2-} results from the oxidation to sulphuric acid in liquid clouds, primarily by H_2O_2 and O_3. In the current stable model version (EMEP rv1.1, see section 2.2) we use an oxidation rate which represents both oxidation in gas phase and in the aqueous phase. This reaction rate was, however, developed based on observations in the 1980's (Eliassen and Saltbones, 1983). The changes in the SO_2 emissions over the last twenty years have lead to changes in the pH in cloud water, and this have probably lead to changes in the production of SO_4^{2-} by the O_3 pathway. Especially in the source regions, the reduced SO_2 emissions would tend to increase the fraction of SO_2 that is oxidised.

As a sensitivity test, we increased both the average mean value and the amplitude of the sine function representing the oxidation rate with 25%. The result is shown in Table 4.1. Scatter plots for SO_2 and SO_4^{2-} resulting from the sensitivity test are given in figures 4.2(top) and 4.4(top) and can be compared to the base case in figures 4.1(top) and 4.3(top). The yearly average SO_4^{2-} concentration in air increased by 13% from 0.61 μg(S)/m^3 to 0.69 μg(S)/m^3 (Observations: 0.72 μg(S)/m^3). Since SO_2 has a shorter residence time in the atmosphere than SO_4^{2-}, the SO_2 concentration change less than SO_4^{2-}, from 1.97 μg(S)/m^3 to 1.91 μg(S)/m^3 (Observations 1.04 μ g(S)/m^3). The increased oxidation rate gives results that are better in agreement with the observations, both for SO_2 and SO_4^{2-}, indicating a somewhat too low oxidation rate in the current version of the EMEP Unified model. Further investigations will be made to try to find a better methodology for the SO_2 oxidation.

a) Reference case

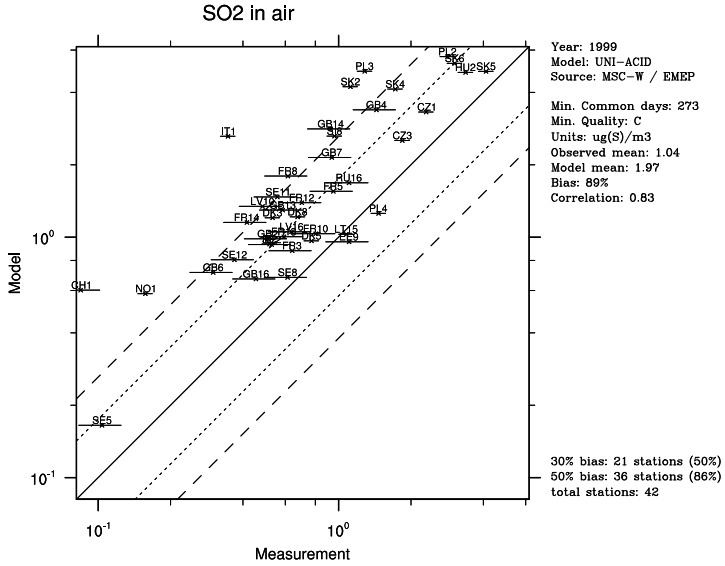

b) V_g increased 50%

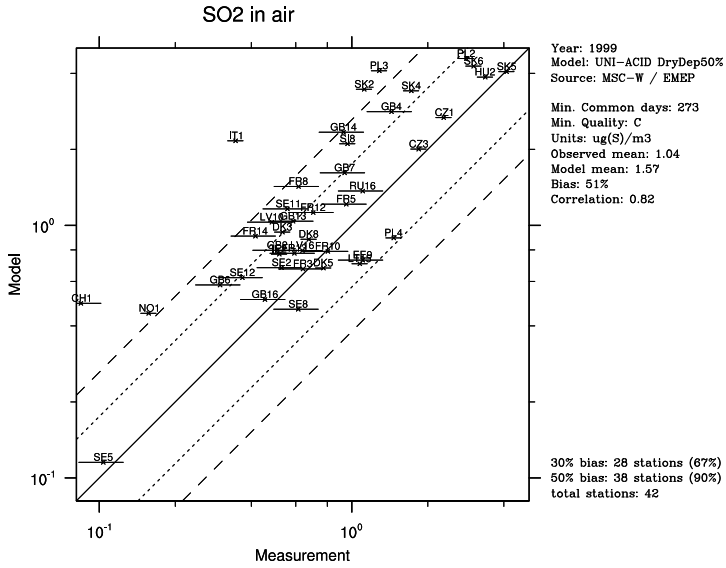

Figure 4.1: Modelled versus observed results for SO_2 in air (μg(S)m^{-3}) for 1999: Annual average for all stations with expected data uncertainty (reported by CCC) $< 30\%$ and measurements for at least 75% of the days. Results of reference case and the sensitivity test where the dry deposition velocity for SO_2 is increased with 50% (see text).

a) Ox. rate increased 50 percent

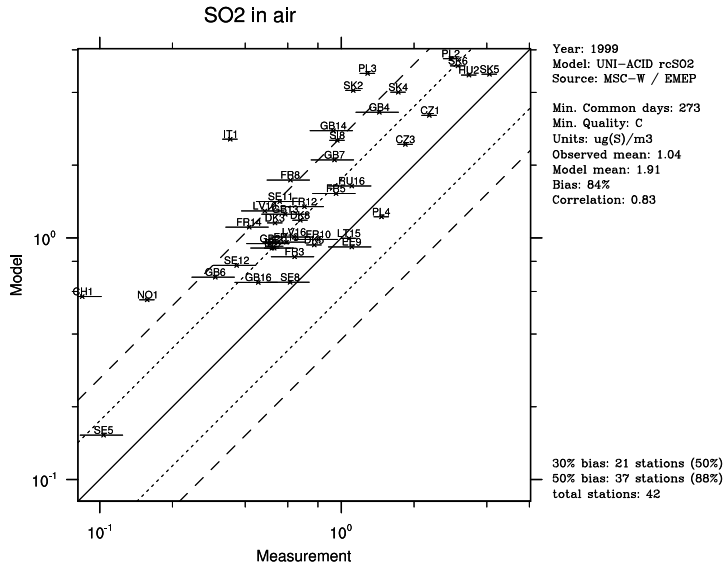

b) High SO_2 emissions

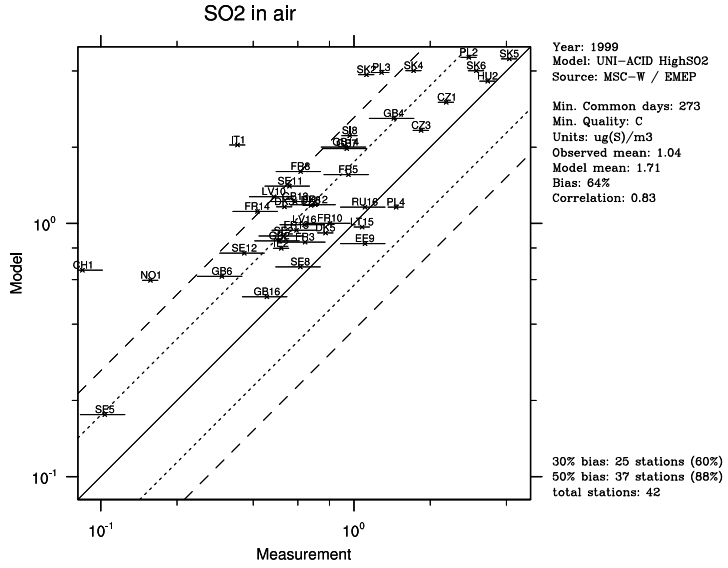

Figure 4.2: Modelled versus observed results for SO_2 in air (μg(S)/m^3) for 1999: Annual average for all stations with expected data uncertainty (reported by CCC) $<$ 30% and measurements for at least 75% of the days. Results of the sensitivity tests where (upper figure) the oxidation rate for SO_2 to SO_4^{2-} is increased with 25% and (lower figure) all the SO_2 emissions are released in model layer 4 ($\approx$ 400 meters).

a) Reference case

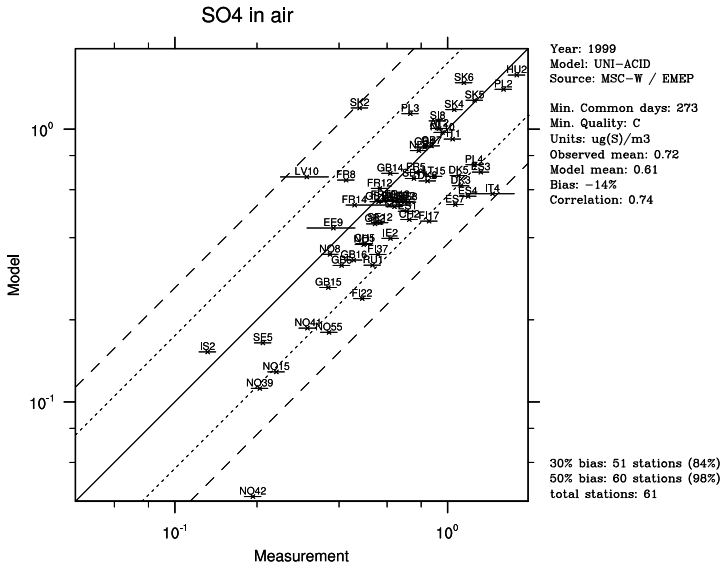

b) V_g increased 50%

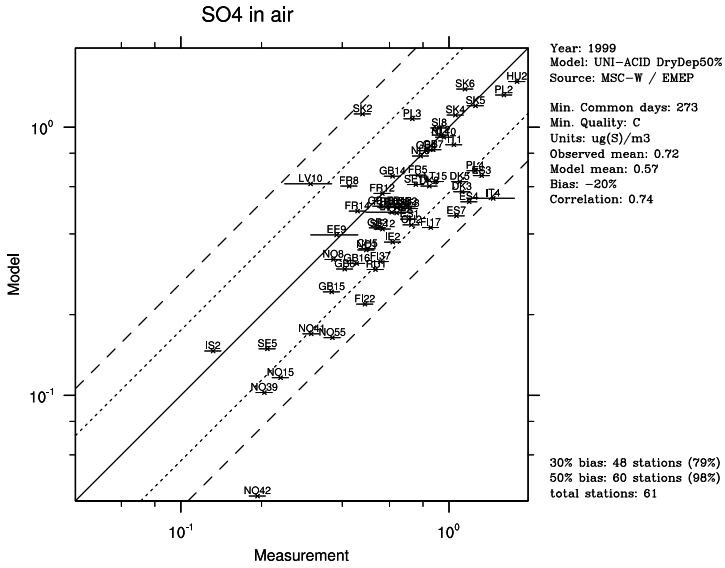

Figure 4.3: Modelled versus observed results for total sulphate in air (μg(S)m^{-3}) for 1999: Annual average for all stations with expected data uncertainty (reported by CCC) $< 30\%$ and measurements for at least 75% of the days. Results of reference case and the sensitivity test where the dry deposition velocity for SO_2 is increased with 50% (see text).

a) Ox. rate increased 50 percent

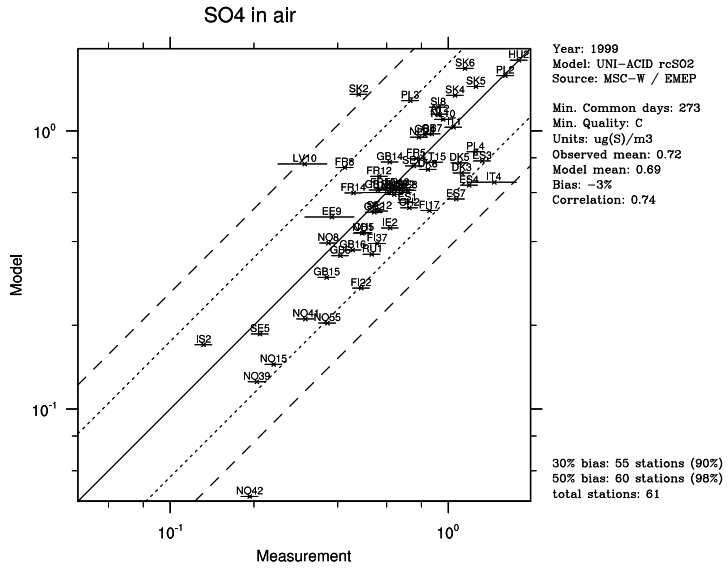

b) High SO_2 emissions

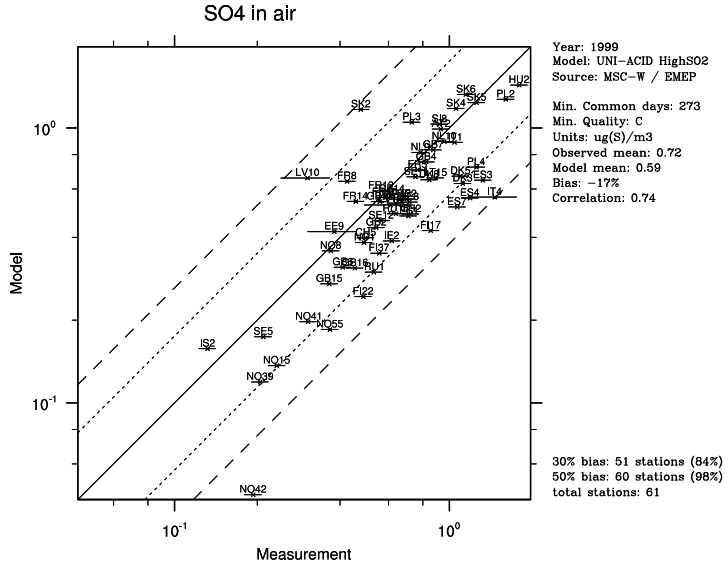

Figure 4.4: Modelled versus observed results for total sulphate in air (μg(S)/m^3) for 1999: Annual average for all stations with expected data uncertainty (reported by CCC) $< 30\%$ and measurements for at least 75% of the days. Results of the sensitivity tests where (upper figure) the oxidation rate for SO_2 to SO_4^{2-} is increased with 25% and (lower figure) all the SO_2 emissions are released in model layer 4 ($\approx$ 400 meters).

a) Reference case

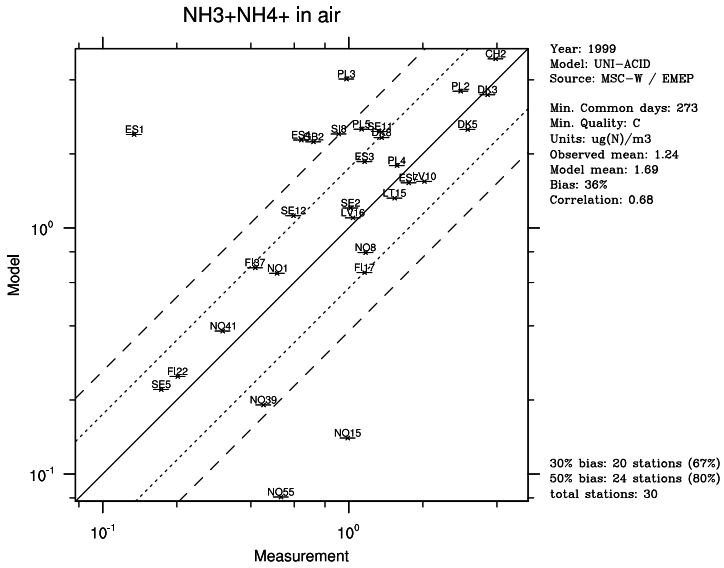

b) $(NH_4)_2SO_4$

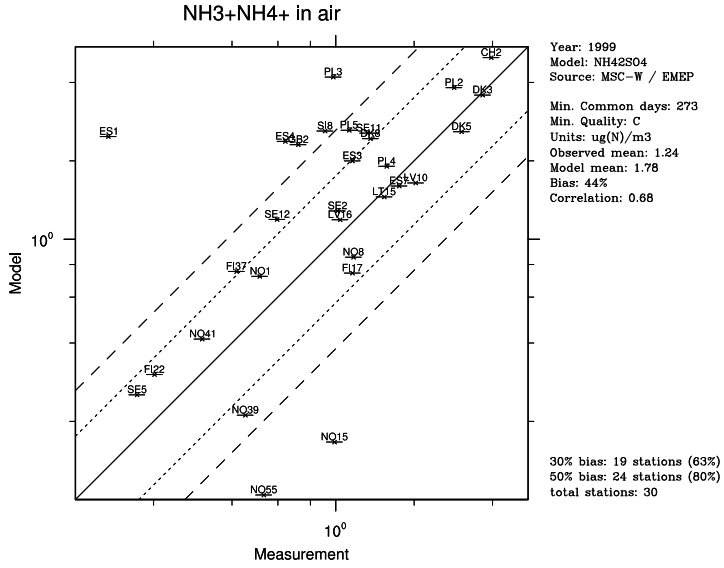

Figure 4.5: Modelled versus observed results for $NH_3 + NH_4^+$ in air (μg(N)/m^3) for 1999: Annual average for all stations with expected data uncertainty (reported by CCC) $< 30\%$ and measurements for at least 75% of the days. Results of reference case and the sensitivity test where the NH_4^+ to SO_4^{2-} in $(NH_4)_xSO_4$ has been increased from 1.5 to 2 (see text).

a) Reference case

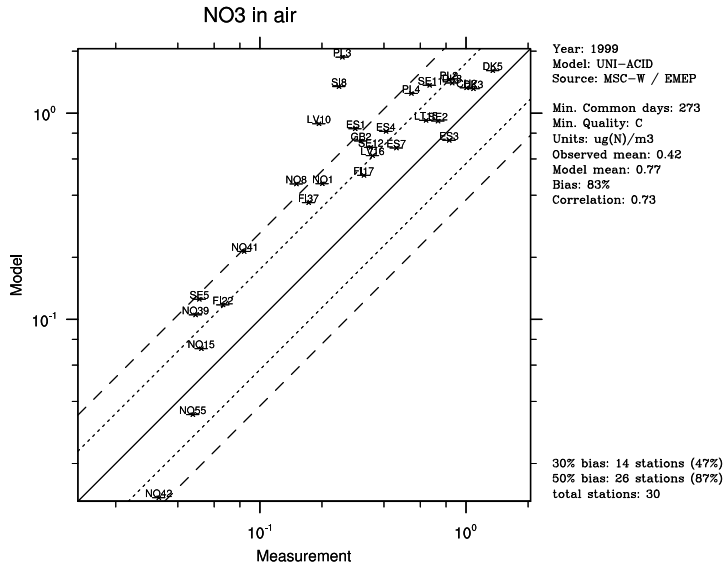

b) $(NH_4)_2SO_4$

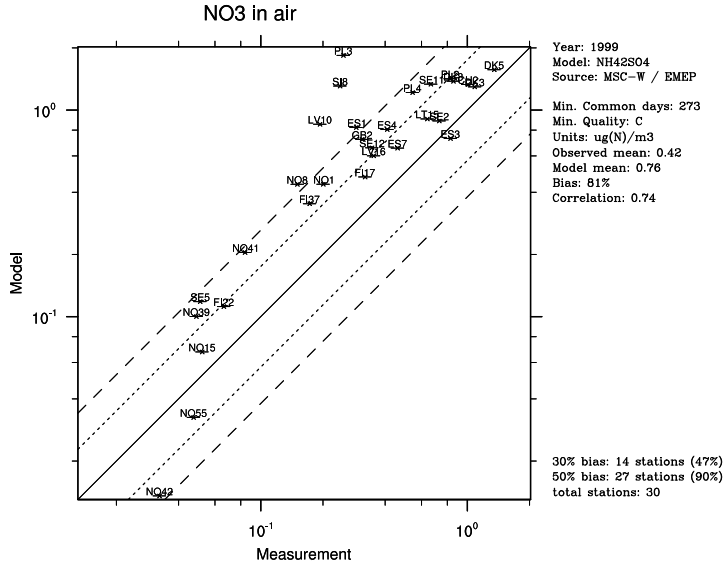

Figure 4.6: Modelled versus observed results for NO_3^-+HNO_3 in air (μg(N)/m^3) for 1999: Annual average for all stations with expected data uncertainty (reported by CCC) $< 30\%$ and measurements for at least 75% of the days. Results of reference case and the sensitivity test where the NH_4^+ to SO_4^{2-} ratio in $(NH_4)_xSO_4$ has been increased from 1.5 to 2 (see text).

4.1.3 Height of SO_2 Emissions

European sulphur dioxide emissions have shown a clear downward trend in recent decades. However, emissions from low level sources and high stack sources have been reduced at different rates in different periods. For example, in the UK, SO_2 emission reductions between 1970 and 1990 resulted from a transition from solid and liquid fuels with high sulphur content to low sulphur natural gas. In addition, the sulphur content in liquid fuels decreased. These changes had the largest influence on the low-level sources (NEG, 2001). In UK in the 1990's, the implementation of integrated pollution control on large plants and the de-regulation of gas use in electricity generation lead to the largest reductions for high sources.

Little detailed information on the height of the emissions sources in Europe is available. Moreover, gases ejected from e.g. power stations have large exit velocities and high temperatures and therefore the effective heights are a lot higher than the stack heights. Since the plume rise is not treated explicitly in the model, we assume effective heights.

In our model calculations, we use a height distribution different for each source sector. Most SO_2 emissions originates from combustion in energy and transformation industries (SNAP level 1) and combustion in manufacturing industry (SNAP level 3). The default distribution for SNAP level 1 to model layers 1-4 from the ground is 10%, 20%, 30%, 40%, where the mid point in model layer 4 is approximately 400 meters. For SNAP level 3, the default distribution is 50% to model layer 1 and 50% to model layer 2.

The above factors and assumptions necessarily introduce an uncertainty in the results. In this section we investigate the sensitivity of the surface SO_2 concentrations to the model input height of SO_2 emissions.

The model was rerun with the distribution for SNAP level 1 and 3 set to 100% emissions in model layer 4. Table 4.1 show the results for 1999 calculated with the default height distribution (column "Reference") and the sensitivity test (column "Emis"). Scatter plots for SO_2 and SO_4^{2-} resulting from the sensitivity test are given in figures 4.2(bottom) and 4.4(bottom) and can be compared to the base case in figures 4.1(top) and 4.3(top). The yearly average SO_2 concentration in air decreased with only 13 %, from 1.97 μg(S)m^{-3} to 1.71 μg(S)m^{-3}. In the night, the boundary layer often sinks to 100-200 meters or below, and the emission release in the sensitivity test is well above the mixing height. However, the emissions are still within the diurnal maximum height of the boundary layer, and most emissions are mixed down to the ground during the day. Therefore, concentrations at the ground are not very sensitive to the height distribution of the emissions, as long as they are within the day time boundary layer height. It should be noted, however, that e.g. a much larger reduction for high sources than for low sources may change the partitioning between the wet and dry sulphur deposition.

4.2 Sensitivity of NO_2 to Background Values of O_3 and OH

In the UNI-ACID version of the EMEP model, we calculate the chemical evolution of only nine components. NO_2 undergoes chemical reactions with O_3, OH and CH_3COO_2,

Component	Obs.	Reference (corr.)	rc1.25 (corr.)	V_g×1.5 (corr.)	Emis. (corr.)
μg m^{-3}					
SO_2	1.04	1.97 (83%)	1.91 (83%)	1.57 (82%)	1.71 (83%)
SO_4	0.72	0.61 (74%)	0.69 (74%)	0.57 (74%)	0.59 (74%)
NO_2	2.03	1.86 (73%)	1.86 (73%)	1.86 (73%)	1.71 (74%)
HNO_3+NO_3	0.42	0.77 (73%)	0.76 (74%)	0.76 (74%)	0.76 (74%)
NH_3+NH_4^+	1.24	1.69 (68%)	1.70 (69%)	1.54 (68%)	1.67 (69%)
mg/l					
SO_4(aq)	0.47	0.53 (73%)	0.54 (73%)	0.48 (72%)	0.56 (73%)
NO_3(aq)	0.39	0.35 (75%)	0.35 (74%)	0.35 (74%)	0.36 (74%)
NH_3+NH_4^+(aq)	0.43	0.45 (56%)	0.45 (55%)	0.42 (55%)	0.45 (55%)
mgm^{-2}					
Wdep SO_4	449	346 (55%)*	349 (55%)	313 (55%)	364 (55%)
Wdep NO_3	369	231 (53%)*	230 (53%)	230 (53%)	232 (52%)
Wdep NH_3+NH_4^+	417	295 (32%)*	296 (32%)	276 (31%)	294 (31%)

Table 4.1: Modelled versus observed results for 1999: Annual average for all stations with expected data uncertainty (reported by CCC) < 30% and measurements for at least 75% of the days (concentrations in air) or 25% (compounds in precipitation). Results of reference case and the sensitivity tests (see text). "**rc1.25**": the SO_2 to SO_4 oxidation rate have been increased by 25%. "V_g**1.5**": The dry deposition velocity for SO_2 at 1 meter has been increased by 50%. "**Emis**": All emissions in sector 1 and 3 have been moved to the fourth model layer from the ground, approximately 400 meters.* *Observation and calculations at Ispra differ by approximately a factor of 10, thereby lowering the correlation substantially. If Ispra is removed from the comparison, correlation increases to 75%, 67% and 60% for wet deposition of SO_4^{2-},NO_3 and $NH_3 + NH_4^+$, respectively.*

in addition to photolysis. It is produced in the reaction of NO with ozone, and in the thermal decomposition of PAN. Ozone, hydroxy radicals and peroxy acetyl radicals are not treated explicitly in the Acid Deposition version, but prescribed. We have studied the sensitivity of NO_2 to the choice of background concentrations of two of these components, O_3 and OH.

4.2.1 Prescribed Values of O_3

Two sets of monthly averaged O_3 background fields are applied. The default set is derived from climatological O_3 data published of Logan (1998). Logan use sonde data in combination with surface and satellite data to derive gridded O_3 data of 4 °latitude by 5 °longitude for 13 pressure levels. Both data sets are interpolated to 150×150 km^2 horizontal resolution and to the 20 vertical levels in the EMEP Unified Eulerian model.

As a second dataset, we have obtained O_3 values for 1997 calculated with the global model CTM2 (Sundet, Pers. comm.) from the University of Oslo. The model data has a resolution of 5.625°×5.625° with 19 vertical layers up to 10hPa. In general, the CTM2 model data show higher O_3 concentrations at ground level and up to approximately

6-7 km than the climatology data. In contrast, the O_3 climatology data exceeds the modelled data at higher levels. In the climatology data for the summer season, surface values over sea are given values that are much lower than those over land, based on the argument that ozone values in general are much lower at remote marine locations than at rural sites. Ozone values over the Mediterranean sea are sometimes as low as 20-25 ppb at summer time. However, in the CTM2 data, we generally find the highest ozone values in Europe over the Mediterranean sea, especially near the coast of Greece and Italy. This is also found in the results from the EMEP model.

Despite these relatively large differences in the two O_3 fields, the calculations with UNI-ACID give very similar results for NO_2. For most stations, except were the most extreme differences of the two O_3 sets occur (e.g. Greece), the differences on a day-to-day basis are negligible. The yearly average NO_2 concentration (averaged over all EMEP stations with expected uncertainty $< \pm 30\%$) differ by less than 2% in the two calculations. This shows that the calculations of NO_2 surface concentrations are relatively robust against the choice of O_3 background values.

The likely reason for this is that in UNI-ACID O_3 affects the reaction scheme for NO_2 in only two respects. Firstly, at nighttime O_3 reacts with NO_2 to form HNO_3. At low temperatures the lifetime is long (ca. 12-18 h at 40 ppb ozone, 0-10°C). Moderate differences in O_3 concentration will have little effect on the net loss of NO_2 under these conditions. Secondly, O_3 takes part in the cycle where photolysis of NO_2 produces NO (plus O) and ozone reacts with NO to regenerate NO_2. The characteristic time of this cycle is usually short enough so that a steady state is achieved quickly. In a steady state approximation, $[NO_2]/[NO] = k \cdot [O_3]/J_{NO_2}$. An increase in the ozone background concentration gives a higher $[NO_2]/[NO]$, which is achieved by a decrease (Δ) in the concentration of NO and an equal increase in NO_2. Since [NO] in general is $\ll [NO_2]$, the Δ is small, and the influence on the NO_2 concentrations even less.

4.2.2 Prescribed Values of OH

In the UNI-ACID version of the EMEP model, OH is prescribed by a simple function of the solar zenith angle, Θ, as described in Table 4.2. In addition, OH values below clouds are reduced with a factor of 0.5 times the fractional cloud cover. Results from the UNI-OZONE version of the EMEP model version suggest a marked seasonal variation of OH with much higher daily maximum values for OH in the summer than the concentrations assumed in the UNI-ACID version. As a sensitivity test, we implemented a seasonal variation of the OH concentrations, with clear sky summer maximum ($\approx 1.2 \cdot 10^7$molecules cm^{-3}) and winter minimum ($\approx 10^6$molecules cm^{-3}) set to match the results from the EMEP Unified Photo-oxidant model version calculations.

Results for 1999 using the two different functions of prescribed OH concentrations are shown in Table 4.3. Time series for Vavihill, Sweden, with and without the seasonal variation of the OH concentrations are presented in figure 4.7. The average NO_2 concentration decreases, mainly due to increased OH concentrations in summer.

We examined the correlation between model results and the observations in time-series for the 71 EMEP stations with measurements for more than 75% of the days in 1999. Of those, 43 stations were in better agreement with observations, for 8 stations the correlation remained unchanged, whereas 20 stations had lower correlation than in the reference model version. Thus, the correlation between measurements and model

Version	Night	Day
rv1.1	10^4	$10^4+10^6\cdot\exp(-0.25/\cos\Theta)$
Sensitivity test	10^4	$10^4+\text{SEASON}\cdot\exp(-0.25/\cos\Theta)$

Table 4.2: Prescribed concentration of OH in the UNI-ACID version of the EMEP model in molecules cm^{-3} . SEASON=$10^6+1.1\cdot10^7$*sin($\pi\cdot$(366-day)/366)

Component	**Obs.**	**Reference (corr.)**	**OH (corr.)**	$(NH_4)_2SO_4$ **(corr.)**
μg/m^3				
SO_2	1.04	1.97(83%)		
SO_4	0.72	0.61(74%)		
NO_2	2.03	1.86(73%)	1.66(73%)	
HNO_3+NO_3	0.42	0.77(73%)	0.84(73%)	0.76(74%)
NH_3+NH_4^+	1.24	1.69(68%)	1.72(69%)	1.78(68%)
mg/l				
SO_4(aq)	0.47	0.53(73%)		
NO_3(aq)	0.39	0.35(75%)	0.38(75%)	0.35(74%)
NH_3+NH_4^+(aq)	0.43	0.45(56%)	0.45(55%)	0.47(56%)
mgm^{-2}				
Wdep SO_4	449	346(55%)*		
Wdep NO_3	369	231(53%)*	248(53%)	229(53%)
Wdep NH_3+NH_4^+	417	295(32%)*	298(32%)	312(32%)

Table 4.3: Modelled versus observed results for 1999: Annual average for all stations with expected data uncertainty (reported by CCC) $<$ 30% and measurements for at least 75% of the days (concentrations in air) or 25% (compounds in precipitation). Results of reference case and the sensitivity tests (see text). * *Observation and calculations at Ispra differ by approximately a factor of 10, thereby lowering the correlation substantially. If Ispra is removed from the comparison, correlation increases to 75%, 67% and 60% for wet deposition of* SO_4^{2-},NO_3 *and* $NH_3 + NH_4^+$, *respectively.*

results in general increase when the seasonal variation of the OH concentration is taken into account. The overall effect on the modelled NO_2 concentrations is ,however, fairly small.

4.3 Ratio of NH_4^+ to SO_4^{2-} in $(NH_4)_xSO_4$

Ammonium sulphate may exist in aerosol phase in forms like letovicite ($(NH_4)_3H(SO_4)_2$), NH_4HSO_4, and $(NH_4)_2SO_4$. In the UNI-ACID and UNI-OZONE versions of the EMEP model, we assume a ratio of ammonium to sulphate of 1.5, which correspond to a 75% neutralisation of H_2SO_4. Because SO_2 emissions have decreased whereas NH_3 emissions have remained fairly constant over the last twenty years, we may expect an increasing degree of neutralisation of H_2SO_4 at present relative to earlier years.

The UNI-ACID model was rerun for 1999 with a NH_4^+-to-SO_4^{2-} molar ratio of 2

a)

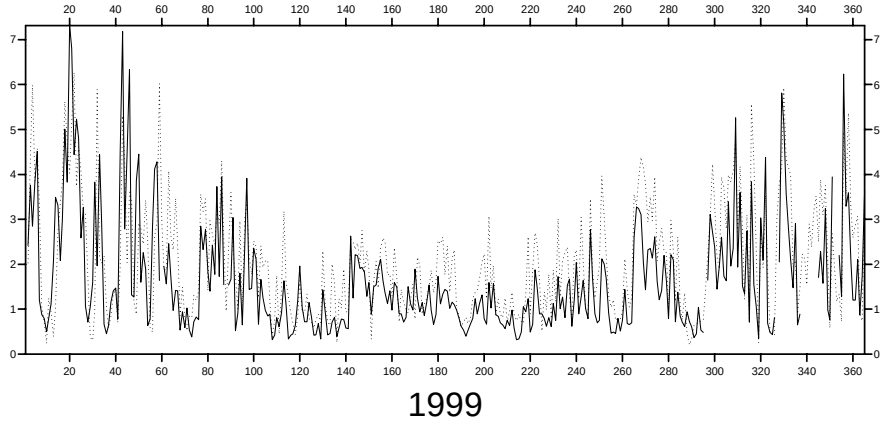

b)

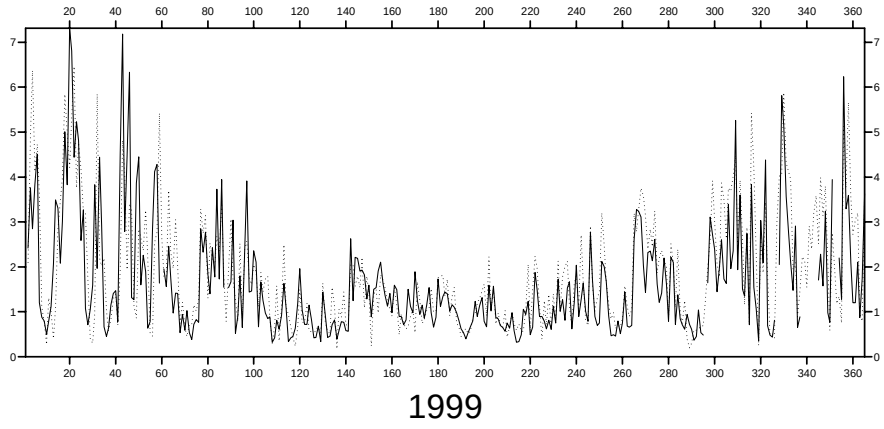

Figure 4.7: Timeseries for modelled (dashed line) and observed (solid line) NO_2 (in μg(N)m^{-3}) at Vavihill, Sweden, using two different functions of prescribed OH (see Table 4.2). a) using calculation with OH as a function of the solar zenith angle. b) with additional seasonal variation of OH, see text.

(fully neutralised sulphate). This is likely to be a good approximation in areas where the NH_3 emissions exceed the air concentration of SO_4^{2-} by more than a factor of 2. Our model calculations predict that this is the case in most of central Europe today.

The results of the sensitivity test is shown in Table 4.3. Scatterplots for NH_3+NH_4^+ in air resulting from the sensitivity test are compared to the base case in figure 4.5. The ammonia+ammonium concentrations in air increase ($\approx$5%) because more NH_3 is converted to NH_4^+, which has a longer residence time in the atmosphere. Scatterplots for total nitrate in air for the base case and for the sensitivity test are shown in figure 4.6. Nitrate concentrations decrease because less NH_3 is available to form NH_4NO_3, but since NH_4NO_3 exist in an equilibrium with NH_3 and HNO_3, the effect is damped. The overall effect is a slight change towards more wet deposition relative to dry deposition.

However, the results show that the degree of neutralisation of SO_4^{2-} due to change of the ratio of NH_4^+ to SO_4^{2-} does not introduce major uncertainties in the model results.

4.4 Conclusions

In this chapter, the sensitivity of the EMEP Unified Acid Deposition model version towards some changes in non-meteorological variables has been studied. In general, we found the model to be fairly robust against changes in the chemistry. The results of the investigation can be summarised in the following points:

- The uncertainties in modelling of SO_2 dry deposition velocities have a moderate influence on calculated surface concentrations of SO_2. A 50% increase in V_g caused a 20% reduction in surface concentrations.
- Modelled SO_2 concentrations are relatively robust with respect to uncertainties in SO_2 emission heights, at least for the limited tests conducted here.
- The SO_2 to SO_4^{2-} oxidation rate in the current model is probably somewhat low, but a large increase in the oxidation rate is necessary to change the results substantially.
- Modelled NO_2 concentrations are robust against the choice of background O_3 field, as long as the O_3 field is reasonable.
- The choice of background OH field has a minor influence on the modelled NO_2 concentrations. However, the correlation between observations and modelled NO_2 concentrations may be (slightly) improved by including a seasonal variation for OH background concentrations.
- Concentrations of nitrate and ammonia+ammonium in air are relatively robust to the partitioning between $(NH_4)_3H(SO_4)_2$, NH_4HSO_4, and $(NH_4)_2SO_4$ in the model.

4.5 References

Eliassen, A. and Saltbones, J. , 1983, Modelling of long-range transport of sulphur over europe: A two year model run and some model experiments., *Atmospheric Environment*, 22, 1457–1473.

Fowler, D. , Sutton, M. A. , Flechard, C. , Cape, J. N. , Storeton-West, R. , Coyle, M. , and Smith, R. I. , 2001, The control of SO_2 dry deposition on to natural surfeces by NH_3 and its effects on regional deposition, *Water, Air and Soil Pollution*, 1, 39–48.

Logan, J. A. , 1998, An analysis of ozonesonde data for the troposhere: Recommendations for testing 3-d models and development of a gridded climatology for troposheric ozone, *J. Geophys. Res.*, 10, No. D13, 16,115–16,149.

2001, Transboundary air pollution: Acidification, eutrophication and ground-level ozone in the UK, Technical report.

Chapter 5

Modified Parametrisation for Vertical Diffusion

Hilde Fagerli and Anton Eliassen

Previously, the Eulerian modelling tools at EMEP MSC-W consisted of two main models, the acidification model (MADE) (Berge and Jakobsen, 1998, Jonson et al., 1998b) and the oxidant model (MACHO) (Jonson et al., 1997, Jonson et al., 1998a). In the process of "unifying" the model systems, it was discover that the vertical mixing in the atmospheric boundary layer was too inefficient, particularly under stable conditions and under conditions approaching free convection. In addition, several programming errors were discovered. This made it necessary to reevaluate and modify the treatment of vertical diffusion in the model.

This chapter discusses the modified vertical diffusion scheme that has been implemented in the unified EMEP Unified Eulerian model up to July 2002. This work will be continued in the autumn of this year.

5.1 Vertical Diffusion in Earlier Versions of EMEP MSC-W Eulerian Models

The vertical sub grid turbulent transport is modelled as a diffusive effect. The turbulent diffusivity coefficient, K_z, is derived from basic meteorological parameters. The vertical exchange coefficient is given by

$$K_z = l^2 \left| \frac{\Delta v_H}{\Delta z} \right| F(Ri) \tag{5.1}$$

The turbulent mixing length, l, is parameterised according to Nordeng (1979)

$$\begin{aligned} l &= \kappa \cdot z \quad && z \leq z_m \\ l &= \kappa \cdot z_m \quad && z > z_m \end{aligned}$$

where κ is the von Karman constant (κ=0.35), z is the height above the ground and z_m=200 m. The local, bulk Richardson number in the layer of thickness Δz is defined as

$$Ri = \frac{g}{\Theta} \cdot \frac{\left(\frac{\Delta\Theta}{\Delta z}\right)}{\left(\frac{\Delta\overrightarrow{v_H}}{\Delta z}\right)^2} = \frac{g \cdot \Delta z \cdot \Delta\Theta}{\Theta \cdot \left(\Delta\overrightarrow{v_H}\right)^2}$$

where Θ is potential temperature and $\overrightarrow{v_H}$ is the horizontal wind speed. The vertical shear in horizontal wind is given by

$$\left(\Delta\overrightarrow{v_H}\right)^2 = |\Delta\overrightarrow{v_H}|^2 = (\Delta u)^2 + (\Delta v)^2$$

where for an arbitrary state variable q, $\Delta q = q(z + \Delta z) - q(z)$.
Following Nordeng (1979), we assume

$$Ri_c = A \cdot \left(\frac{\Delta z}{\Delta z_0}\right)^B \tag{5.2}$$

where A=0.115, B=0.175 and Δz_0=0.01 m, and

$$F(R_i) = \begin{cases} \sqrt{1.1 - 87 \cdot Ri} & Ri \leq 0 \\ 1.1 - \frac{Ri}{Ri_c} & 0 < Ri \leq 0.5 \cdot Ri_c \\ 1.0 - \frac{Ri}{Ri_c} & 0.5 \cdot Ri_c < Ri < Ri_c \\ 0.001 & Ri \geq Ri_c \end{cases} \tag{5.3}$$

In sigma coordinates, the diffusion coefficient has the following form:

$$K_\sigma = K_z \cdot \rho^2 \cdot \left(\frac{g}{p^*}\right)^2$$

The scheme given above is applied to the free troposphere, above the mixing height. In the boundary layer below the mixing height we have implemented a modified formulation of vertical diffusion, see section 5.3 below.

5.2 Estimation of Atmospheric Boundary Layer Height

In the EMEP Unified model, we have implemented an estimation of the atmospheric boundary layer height based on data available from numerical weather prediction models, rather than on observational data. Two different schemes are used, depending on the direction of the turbulent heat transport in the surface layer. In the stable case when the turbulent heat flux is directed downwards, a strong horizontal wind may nevertheless produce mechanical turbulence, if the Richardsons number is large enough. Thus following equation 5.1,5.2 and 5.3, the vertical turbulent exchange coefficient (K_z) is calculated on the basis of the local Richardson number at every level. The height of the ABL in this case is taken as the height of the lowest level above 100 m where K_z is smaller than 1 $m^2 s^{-1}$. If the ABL as a whole is unstable, the turbulent heat flux is directed upwards from the ground to the atmosphere. The heating from below will initiate convective mixing which can be very efficient if the heating is strong. The convective mixing will cause the potential temperature in the ABL to be close to constant with height, thus following a dry adiabat. As the heating continues, the potential temperature will grow with time along with the thickness of the layer which is being convectively adjusted in the process. We assume an adjustment time for distribution

of heat throughout the ABL of one hour. Thus depending on the initial distribution of the potential temperature, the height of the unstable ABL is calculated as the thickness of the layer above the ground for which the change in the internal energy equals the heat input from the ground over one hour. Since both this thickness and the final temperature initially are unknown, this is done by stepping level by level in the vertical direction calculating the increment in internal energy for the layer (i.e. consisting of several layers) between the ground and the final level where the total change in internal energy equals the heat input from the ground. Finally, the ABL height is smoothed with a second order Shapiro filter in space (Shapiro, 1970). The ABL height is not allowed to be less than 100 m or exceed 3000 m.

Figures 5.1 and 5.2 show the calculated ABL heights in January and July 1999 based on data from HIRLAM. In the winter time, low solar radiation provides conditions for a thin and stable ABL over the continent. A gradual increase in calculated ABL heights southward over land is evident. The diurnal variation is small over the continent. In the summer, daytime continental ABL heights are larger than over the sea due to the turbulent heat transport from the ground in the surface layer over the continent. Figure 5.2 demonstrates a strong diurnal cycle in mixing heights caused by solar radiation, with a thin and stable ABL over the continent at night (rarely above 400m) and boundary heights between 1000-2000m at mid-day.

The boundary layer heights calculated using the HIRLAM data thus behaves as expected. In the Lagrangian EMEP model mixing heights were estimated from regular radiosonde instead. So far, we have not made any comparison between "observed" and calculated mixing heights, but the behaviour of the two sets of mixing heights seems to be similar.

5.3 Formulation of Vertical Diffusion in the Boundary Layer

In the unstable case, K_z is determined by the O'Brien (1970) profile:

$$K_z(z) = K_z(z_i) + \left(\frac{z_i - z}{z_i - h_s}\right)^2 \Big\{ K_z(h_s) - K_z(z_i) + (z - h_s) \cdot \left[\frac{\delta}{\delta z}(K_z(h_s)) + 2 \cdot \frac{K_z(h_s) - K_z(z_i)}{z_i - h_s}\right] \Big\} \qquad h_s \le z < z_i$$

in which z_i is the mixing height and h_s is the height of the surface boundary layer (or the so-called constant flux layer). In the model calculation h_s is set to 4% of the mixing height z_i. From the similarity theory of Monin and Obukov for the surface layer (see for example Stull (1988) for a description of this theory) we have

$$K_z(z) = \frac{u_* \cdot \kappa \cdot z}{\Phi\left(\frac{z}{L}\right)} \tag{5.4}$$

where κ is the von Karman constant and Φ is a universal function. The Monin-Obukov length is given by the turbulent fluxes of momentum τ and heat H

$$L = \frac{\theta \cdot u_*^2}{\kappa \cdot g \cdot \theta_*}$$

a) 00 UTC

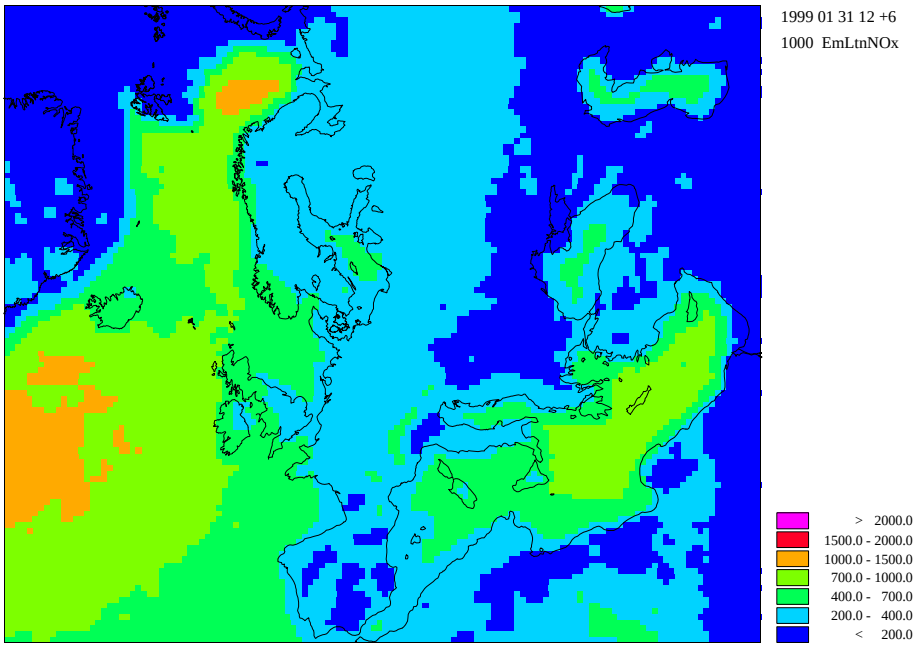

b) 12 UTC

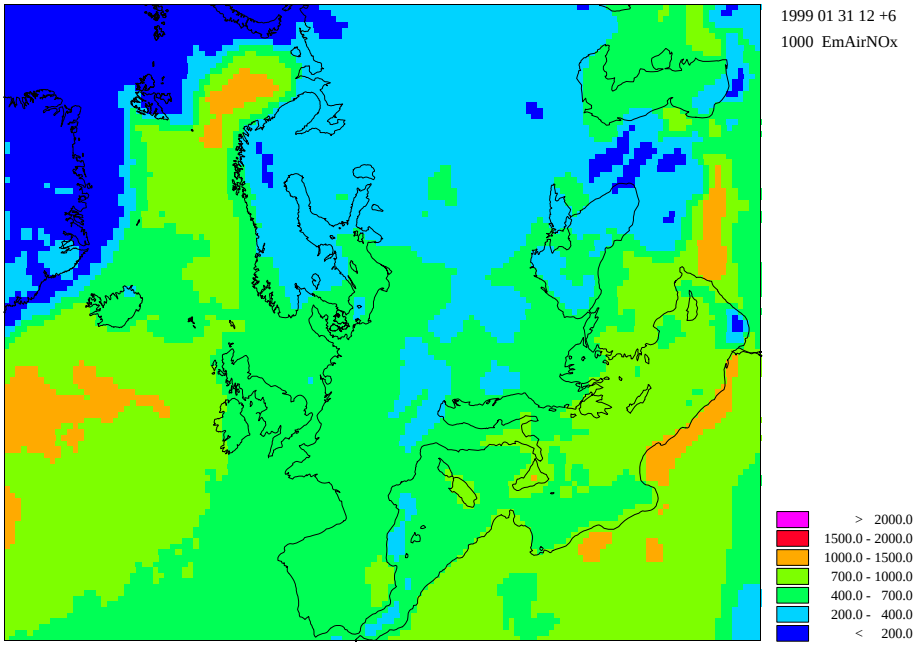

Figure 5.1: Average mixing layer height (m) at a) 00 UTC and b) 12 UTC for January 1999.

a) 00 UTC

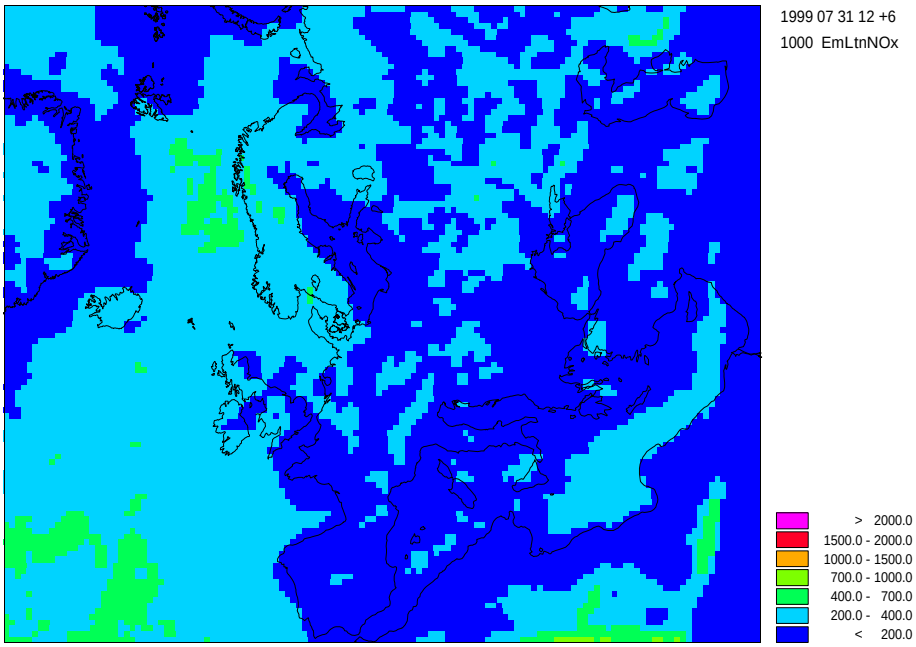

b) 12 UTC

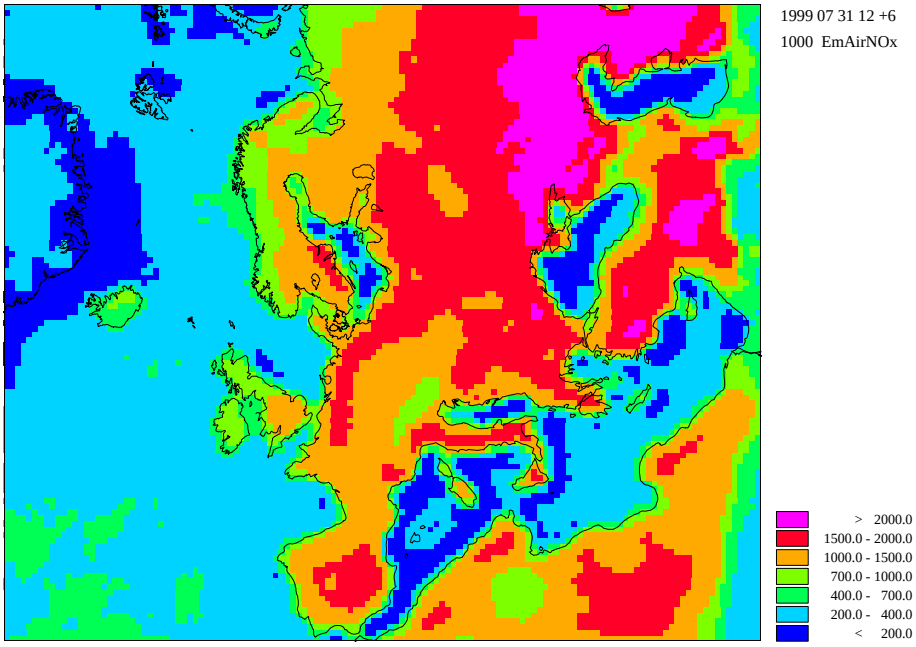

Figure 5.2: Average mixing layer height (m) at a) 00 UTC and b) 12 UTC for July 1999.

where

$$-u_*\theta_* = \frac{H}{C_p \cdot \rho}$$

and

$$\frac{\tau}{\rho} = u_*^2$$

H and τ are taken from the HIRLAM NWP model.
For Φ we assume;

$$\Phi\left(\frac{z}{L}\right) = \begin{cases} \frac{0.74}{\left(1-9\cdot\left(\frac{z}{L}\right)\right)^{1/2}}, & z/L \geq -2 \\ \frac{0.74}{\left(1-\alpha\cdot\left(\frac{z}{L}\right)\right)^{1/3}}, & 0 < z/L < -2 \end{cases} \tag{5.5}$$

with

$$\alpha = \frac{1}{2}\left(\sqrt{6859} - 1\right) \approx 40.9$$

The formula for $z/L \geq -2$ is taken from Businger et al. (1971), while the second one is taken from Iversen and Nordeng (1987).

In the stable case, $K_z(z)$ is calculated using equations 5.1,5.2 and 5.3. To avoid non physically small exchange coefficients within the boundary layer, we introduce a minimum K_z for turbulent exchange between model layers below the mixing height, given by (5.4) and evaluated at the top of the lowest model layer i.e. at z ≈90 meters. In the unstable SBL, we use the universal functions in equation 5.5, whereas in the stable surface layer, we use

$$\Theta(\frac{z}{L}) = 0.74 + 4.7 \cdot (\frac{z}{L}) \ , L > 0 \tag{5.6}$$

Figure 5.3 shows time series of NO_2 for Birkenes, 1999, obtained with the UNI-ACID model (rv1.0, see section 2.2), but with the different schemes for vertical diffusion described in this chapter. The figure at the top is the time series obtained using equations 5.1,5.2 and 5.3 (a), whilst the second figure shows results from a calculation with the new parametrisation (b). The overall effect is a decrease in NO_2 concentrations. The improvement for SO_2 is not as pronounced as for NO_2. Further work to evaluate the presently used vertical concentration profiles in the surface layer remains, however.

5.4 References

Berge, E. and Jakobsen, H. A. , 1998, A regional scale multi-layer model for the calculation of long-term transport and deposition of air pollution in Europe, *Tellus*, 50, 205–223.

Businger, J. A. , Wyngaard, J. C. , Izumi, Y. , and Bradley, E. F. , 1971, Flux-profile relationship in the atmospheric boundary layer, *J. of Atmospheric Sciences*, 28, 181–189.

(a) Old K_z

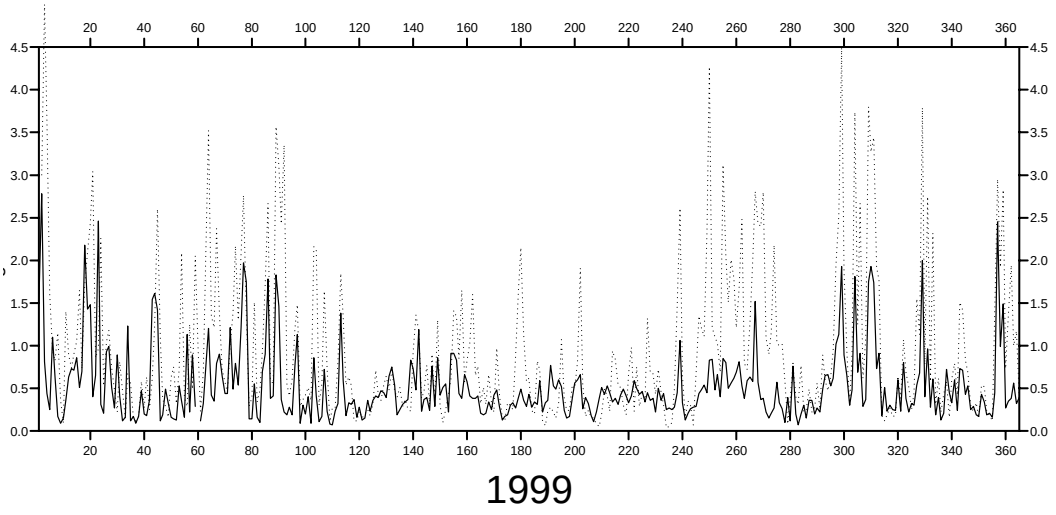

(b) New K_z

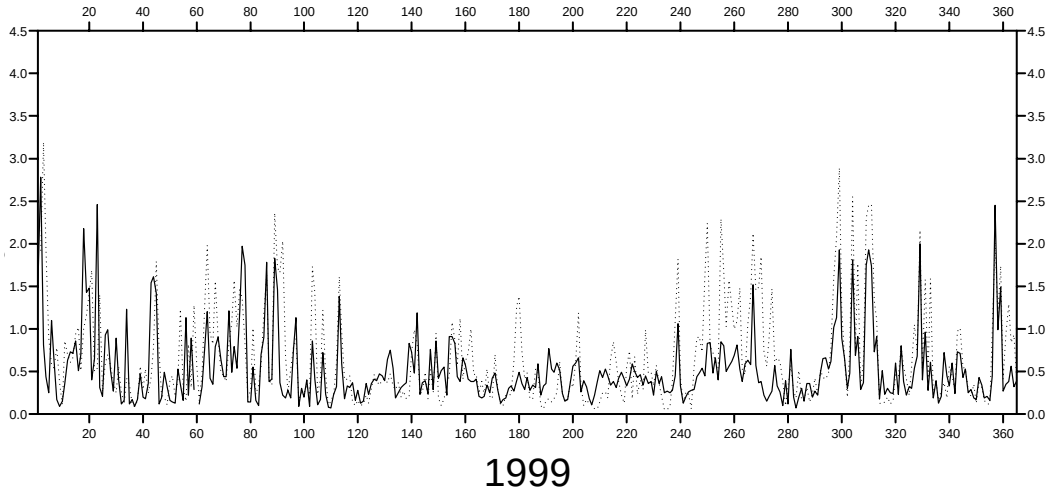

Figure 5.3: Time series for modelled versus observed NO_2 concentrations (μg(N)m^{-3}) at Birkenes, 1999, with old and new formulations for K_z (see text). Results obtained with EMEP model (UNI-ACID, rv1.0)

Iversen, T. and Nordeng, T. E. , 1987, A numerical model suitable for the simulation of a broad class of circulation systems on the atmospheric mesoscale, Technical Report 2, Norwegian Institute for Air Research.

Jonson, J.E. , Jakobsen, H.A. , and Berge, E. , 1997, Status of the development of the regional scale photo-chemical multi-layer Eulerian model, Norwegian Meteorological Institute, EMEP MSC-W Note 2/97.

Jonson, J. E. , Tarrasón, L , Sundet, J.K. , Berntsen, T. , and Unger, S. , 1998a, The Eulerian 3-D oxidant model: Status and evaluation for summer 1996 results and

case-studies, In *Transboundary photo-oxidant air pollution in Europe.* EMEP/MSC-W Status Report 2/98, The Norwegian Meteorological Institute, Oslo, Norway.

Jonson, J.E. , Bartnicki, J. , Olendrzynski, K. , Jokobsen, H.A. , and Berge, E. , 1998b, EMEP Eulerian model for atmospheric transport and deposition of nitrogen species over Europe, *Environmental Pollution*, 102, 289–298.

Nordeng, T. E. , 1979, Parametrization of physical processes in a three dimensional numerical weather prediction model, Technical Report 65, Norwegian Meteorological Institute, Oslo, Norway.

O'Brien, J. J. , 1970, A note on the vertical structure of the eddy exchange coefficient in the planetary boundary layer, *J. of Atmospheric Sciences*, 27, 1213–1215.

Shapiro, R. , 1970, Smoothing, filtering and boundary effects., *Rev. Geophys. Space Phys.*, 8, 359–387.

Stull, R.B , 1988, *An Introduction to Boundary Layer Meteorology*, Kluwer Acad. Publ., Dordrecht.

Chapter 6

Numerical Non-Linearities in Source-Receptor Relationships

Leonor Tarrasón, Åsmund Ukkelberg and Peter Wind

The numerical representation of transport in Eulerian models introduces different errors that affect the accuracy of the results and in particular, the ability of Eulerian models to provide source allocation estimates. These numerical errors are well recognised and their impact in air quality calculations has been documented also within EMEP.

The theoretical difficulties of Eulerian models to accurately determine grid-to-grid allocation were already pointed out by Berge and Tarrasón (1992), under the initial testing of numerical advection routines for use in the EMEP model. Bartnicki (2000) evaluated the ability of the EMEP Eulerian model to calculate country-to-country source-receptor matrices. He analysed the effect of chemical and numerical non-linearities, without explicitly distinguishing between them, and concluded that the influence of non-linear effects on country-to-country source-receptor matrices was relatively small compared to other sources of uncertainty in model calculations. The study, however, did not include an evaluation of the errors involved in country-to-grid allocation applications.

In this chapter, we summarise the results from two independent research projects that have allowed us to quantify explicitly the influence of numerical errors on country-to-grid and grid-to-grid allocation calculations. The results from both projects are consistent and indicate that the EMEP Eulerian model, with its present resolution of 50x50km^2, is largely appropriate for use in country-to-grid allocation applications at European scale. However, it is not recommended to use this model, or any other Eulerian model independently of the grid resolution, to carry out grid-to-grid allocation calculations.

6.1 Origin of Non-Linearities

Eulerian atmospheric transport models involve different non-linear processes that should be accounted for when studying the effect of emission reductions in air concentrations

and depositions. The origin of these non-linearities may be classified as follows:

- Numerical non-linearities caused by the advection scheme for atmospheric transport,
- Non-linearities inherent in the atmospheric chemistry,
- Non-linearities due to aerosol dynamic processes and their interaction with atmospheric chemistry,

In cooperation with the Centre of Integrated Assessment Modelling (CIAM), MSC-W is presently analysing the influence of each of this type of non-linearities in the calculation of source-receptor relationships by the Eulerian model. The first conclusions from this project, internally called NONLIN, focus on the study of the non-linearities caused by numerical approximations to the atmospheric transport in Eulerian models.

The work on NONLIN has profited from the analysis of the transport routines carried out under a national Norwegian project, in association with NILU, to enable a flexible choice of the grid resolution in the EMEP model (see EMEP/MSC-W, Note 5/2002). Work under this project, internally called NEST, has tested the performance of the Bott advection scheme used in EMEP (Bott, 1989) using different grid resolutions.

The performance of the Bott scheme is usually considered to be quite satisfactory as it is mass-conservative, positive-definite and does not introduce numerical dispersion errors. However, the main drawbacks of the Bott scheme are: 1) the scheme is non-monotonic, that is, it has a tendency to produce new extreme air concentrations and 2) the scheme shows a certain degree of numerical diffusion, that is, it has a tendency to smooth steep gradients. Such errors affect the accuracy of the results and, in both cases, are related to non-linear approximations to the transport equation that affect the ability of the model to produce source allocation calculations.

6.2 Impact of Numerical Errors in Source-Receptor Calculations

In EMEP/MSC-W Note 5/2002 , we have explicitly analysed the numerical errors associated to grid-to-grid

It should be kept in mind that numerical diffusion errors depend on the actual gradient of the concentrations, on the size of the cells (Δx), the length of the time step (Δt), the speed of the wind (u) and on the model used for describing the advection. The dependence on Δx, Δt, and u can be combined to define the Courant number which also defines the criteria for stability in the Bott scheme.

Two different model set-ups have been developed: one running with a grid resolution of 50x50km^2, and the other running with a grid resolution of 10x10 km^2. The model runs are set up with comparable meteorology and emission input data. Two tests have been run to illustrate the problems related to the calculation of atmospheric dispersion from individual sources or groups of sources.

In the first test, the source area has an actual extent of 50x50km^2. When the dispersion of the tracer is reproduced with the 50km grid resolution model, the source

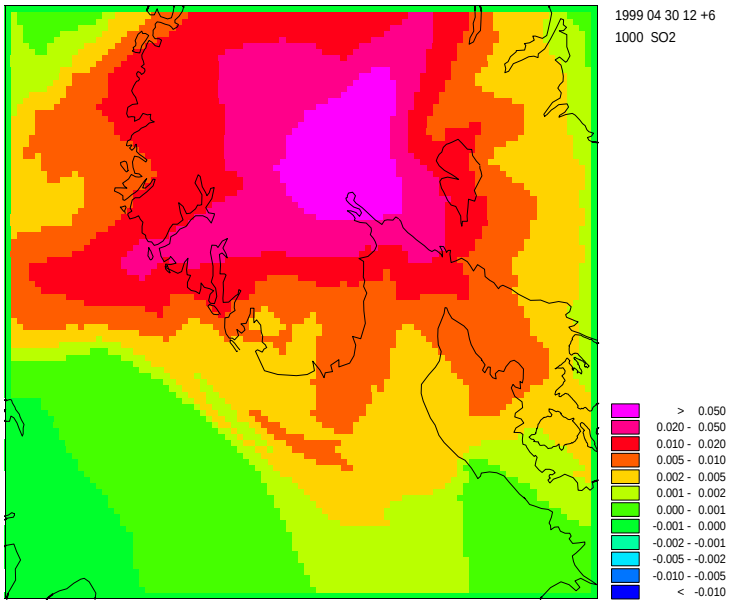

Figure 6.1: Concentration of tracer pollutant($\mu g/m^3$) obtained with the 10km resolution model. Emissions from a 100x100 km^2 source area.

area is resolved using 1 single grid cell. When the tracer dispersion is modelled with the 10km grid resolution model, the source area is resolved using a group of 25 gridcells.

In the second test, the source area has an actual extent of 100x100km^2. In this case, the 50km model can resolve the source using 4 grid cells, while the 10km model resolves the source using 100 gridcells.

The results obtained in the 10km grid (figure 6.1) have less numerical errors than the corresponding results obtained in the 50km grid (figure 6.2) and therefore they have been used as reference for calculations done in the 50km grid. The two simulations have been compared by aggregating each cluster of 5x5 cells in the 10 km grid into one 50 km cell (figure 6.3). Since both calculations use similar Courant numbers, differences are in principle caused by the fact that the emission source is better resolved with the fine resolution model.

Numerical diffusion errors are at their largest when there are steep gradients in the concentration levels. Therefore these errors are most important when we consider the transport from one single grid cell, that is, when the resolution of the source is at its minimum.

If we consider instead a group of sources distributed over several grid cells, these problems are considerably reduced. The condition required to reduce numerical errors is to secure that the source distribution can be expressed as a sum of Fourier components, each with a wave-length larger than twice the grid size. For this reason, Eulerian models are better suited to evaluate the impact of pollution sources distributed over areas resolved by 2-4 grid cells or more.

The results from the above mentioned tests confirm this analysis and indicate how large the numerical errors are when the resolution of the source distribution is low.

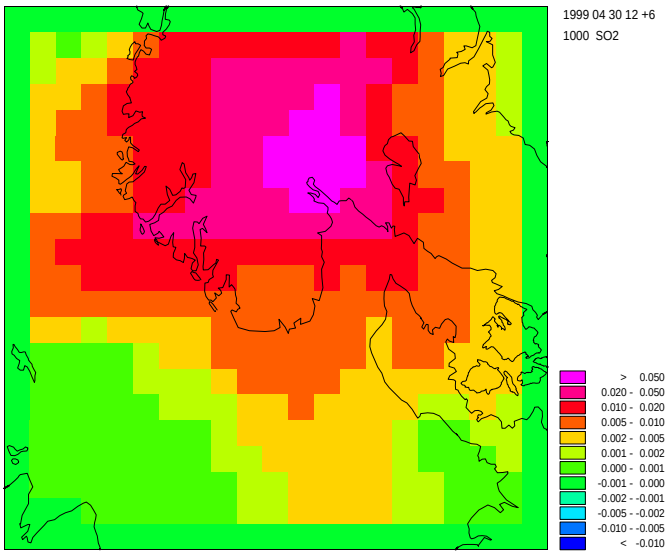

Figure 6.2: Concentration of tracer pollutant($\mu g/m^3$) obtained with the 50km resolution model. Emissions from a 100x100 km^2 source area.

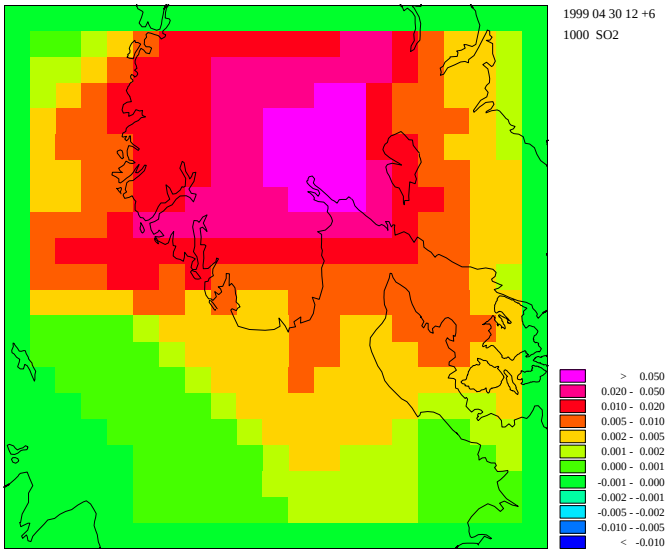

Figure 6.3: Concentration of tracer pollutant($\mu g/m^3$) obtained from a 10km resolution model, aggregated to 50km. Emissions from a 100x100km^2 source area.

When we compared the results from the first test, we observed that largest differences between the 50km simulation and the 10km simulation, could reach up to 50% the concentration values. However, in the second test, when we resolved better the source area, differences in the model runs with different resolutions were in average below 5%, and only in some specific points differences could be up to 15-20% of the concentrations.

6.3 Analysis of Primary Particulate Matter Calculations

Similar results have been obtained through an independent quantification of the effect of numerical non-linearities carried out within the framework of the NONLIN project for primary particulate matter (PPM).

In the NONLIN calculations, primary particles have been considered to be chemically inert. Primary PM has been divided in two different size categories: fine primary particles, PM2.5, with diameters below 2.5μm and coarse primary particles, PMco, with diameters between 2.5μm and 10μm. No coagulation processes have been included in the calculations but the removal of primary particles by dry and wet deposition is size dependent, so that it is possible to distinguish between PM2.5 and PMco removal processes in the calculations Tsyro and Erdman (2000), Tsyro and Tarrasón (2001). These are reasonable assumptions to model PM mass distribution in the atmosphere and imply that the results are free from non-linear effects related to chemical reactions or aerosol dynamic processes.

Therefore, the dispersion of primary particles is suitable for studying the effect and extent of numerical non-linearities in atmospheric transport calculations.

Under the conditions mentioned above, the atmospheric transport and removal of primary particulate matter is a linear function of the PPM emissions and deviations from linearity are only due to the numerical approximations to transport. Thus, numerical non-linearities are simply quantified by establishing the deviation from linearity. In mathematical terms this is expressed as follows:

Consider two different emission scenarios, A and B, for a particular country, k,$e_{A,k}$ and $e_{B,k}$, resulting in the following air concentrations $q_{A,k}$ and $q_{B,k}$. If the model results are linear with respect to emissions then,

$$\frac{q_A}{q_B} = \frac{e_A}{e_B}$$

We can analyse deviations from linearity by comparing the results from model runs from any given scenario, $q_{A,k,\mathrm{run}}$ and $q_{B,k,\mathrm{run}}$ with the results from the following linear estimates:

$$q_{A,k,\mathrm{est}} = \frac{e_{A,k}}{e_{A,k} - e_{B,k}}(q_{A,k,\mathrm{run}} - q_{B,k,\mathrm{run}})$$

and

$$q_{B,k,\mathrm{est}} = \frac{e_{B,k}}{e_{A,k} - e_{B,k}}(q_{A,k,\mathrm{run}} - q_{B,k,\mathrm{run}})$$

If the model results are linear with emissions, then

$$q_{A,k,\mathrm{run}} - q_{A,k,\mathrm{est}} = 0$$

and

$$q_{B,k,\mathrm{run}} - q_{B,k,\mathrm{est}} = 0$$

Deviations from these equations give us a measure of the numerical non-linearities in the results. The two actual scenarios used in the current study are CLE (Current Legislation) and UFR (Ultimate Feasible Reduction) for 2010. Figure 6.4 illustrates the standard procedure used to determine the the extent of numerical non-linearities.

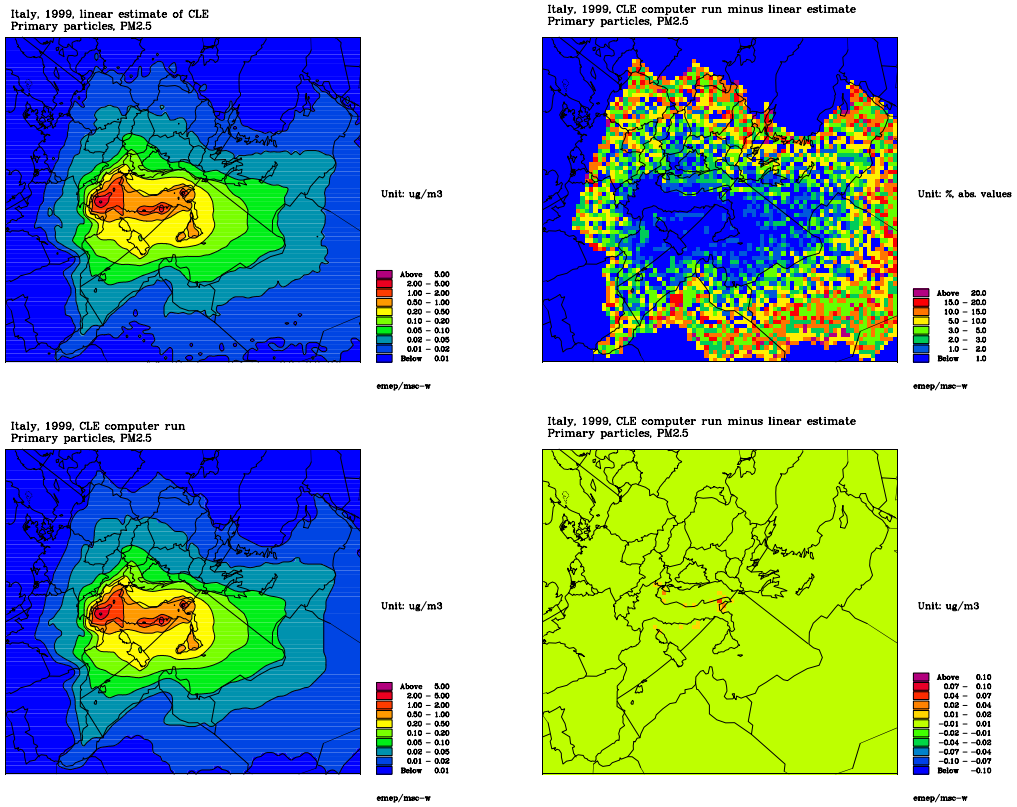

Figure 6.4: Analysis of numerical non-linearities with Italian PM2.5 data as an example. Italian PM2.5 concentrations in CLE scenario (above, left), Linear estimate of the Italian PM2.5 concentrations in CLE scenario (below left), Percentage deviation from the previous figures (above, right) and actual deviations from linearity or numerical non-linearities(below, right).

When interpreting the results from these figures, it is important to differentiate between deviations from linearity caused by the numerical approximations to the transport equation, and deviations caused by round-off or precision errors. The precision of the present model calculations is $0.01\mu g/m^3$, for this reason, we have only analysed deviations from linearity above these limits as significant for the quantification of the numerical effects.

Note that the numerical non-linearities are confined to a limited area around the emitting country and that deviations from linearity occur only in some isolated gridcells. The relative importance of these errors in terms of the total concentration is generally low, between 3-5% and even below. The increase of relative differences at the limits of the plume is only due to the fact that we are calculating percentages related to very low values.

In the following we have evaluated the dependence of these numerical non-linearities with:

- The size fraction of primary PM size fraction: PM2.5 or PMco,
- The meteorological conditions considering both seasonal and diurnal variations,

- The choice of emissions scenario: CLE, MFR or UFR,
- The country or subregion to be studied: United Kingdom, Italy, Germany and The Netherlands.

Dependency on Particle Fraction Coarse particles are effectively removed by dry deposition so that their residence time in the atmosphere is much shorter than for fine particles. Consequently, the travel distances of PMco are shorter than for PM2.5. Since the numerical errors in the model formulation are related to the description of advective transport, we should expect larger non-linearity effects in the PM2.5 concentrations. This is actually the case, as illustrated in figure 6.5. In all tests performed, the spatial extent of numerical non-linearities is consistently larger for fine particles than for coarse particles. For coarse particles, the largest non-linearities are found at very few isolated gridcell in the vicinity of large individual sources and they seldom represent more than 10% of the air concentrations. For fine particles, on the other hand, numerical non-linearities affect areas bordering the country limits, specially in relation with preferred transport directions. Figure 6.5 for fine particles shows an area along the English Channel where non-linear effects are at their largest. This an area where the general gradient in the air concentrations is large due to the transport conditions. Numerical diffusion and monotonicity errors depend on the gradients of air concentrations and are present during the transport giving rise to non-linearities. In any case, these non-linear effects are also small for PM2.5 and seldom represent more that 15% of the concentrations.

Dependency on Season and Time of Day Non-linearity errors have been analysed with 6th hourly resolution for the whole 1999 and the following systematic differences have been identified:

- Diurnal variations: results at 00 GMT and 06GMT (night-time conditions) show larger non-linear behaviour than those at 12GMT and 18GMT (day-time conditions).
- Seasonal variations: results from winter season, October to March, show somewhat larger non-linear effects than results from summer season, from April to September.

The dependence on the time of day is more pronounced than the variations due to season. This is probably related to the stability of the atmosphere and the importance of vertical exchange. Since our analysis is, in first instance, related to air concentrations at surface level, we appreciate a more pronounced effect of numerical diffusion in relation with horizontal advection when there is little vertical exchange. For this reason, under stable conditions in winter nights, the effect of numerical non-linearities becomes slightly larger than otherwise.

Dependency on Choice of Scenario There are apparently differences in the way primary PM2.5 and PMco concentrations respond to emission reductions from the CLE and UFR scenarios. For primary PM2.5 data the deviation from linearity is larger in CLE scenario than in the UFR scenario, whereas for primary PMco data the deviations

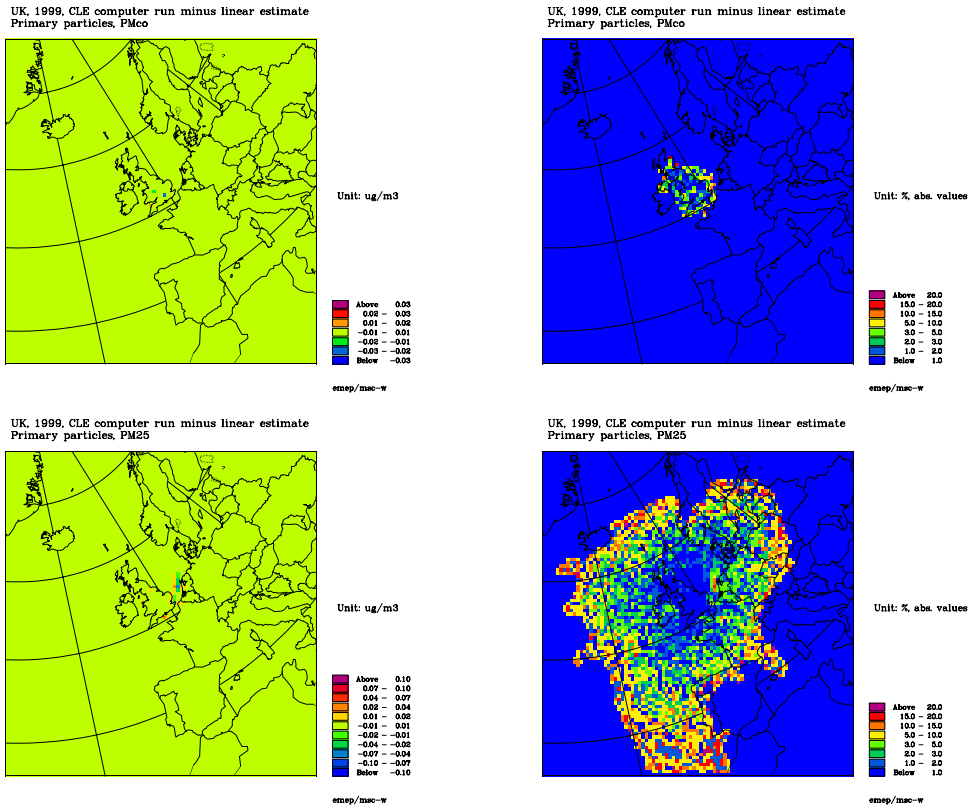

Figure 6.5: Numerical non-linearities associated to the transport of coarse primary particles PMco (above) compared to those associated to the transport of fine particles, PM2.5 (below). Example for UK sources, averaged for 1999.

from linearity are in the CLE scenario are only slightly larger than in the UFR scenarios. This is again consistent with the general dependence of the numerical errors with the concentration gradients but needs to be further investigated in relation with the actual emissions from these scenarios. In order to establish the dependence of numerical non-linearities with the choice of scenario we need to include an additional scenario (MFR) in the analysis. This work is presently under progress.

Dependency on Choice of Country Calculations of atmospheric dispersion of primary particle sources from four different countries have been analysed. For three of them, Germany, United Kingdom and Italy, the influence of non-linear effects is very similar in magnitude. The Netherlands, however, is a relatively smaller country and therefore, we can expect larger numerical errors resulting from transport and somewhat coarser resolution of the country sources in the EMEP grid. Still, the extent of the non-linearities in The Netherlands is not a severe problem. Figure 6.6 illustrates the differences between the results from United Kingdom and The Netherlands. On a yearly average, numerical errors affect the calculation of source allocation for small European countries by introducing up to 10-15% differences between model runs and linear calculations. For most European countries, however, the numerical errors in the calculation of country-to-grid relationships are below 3-5%. These results are reassuring

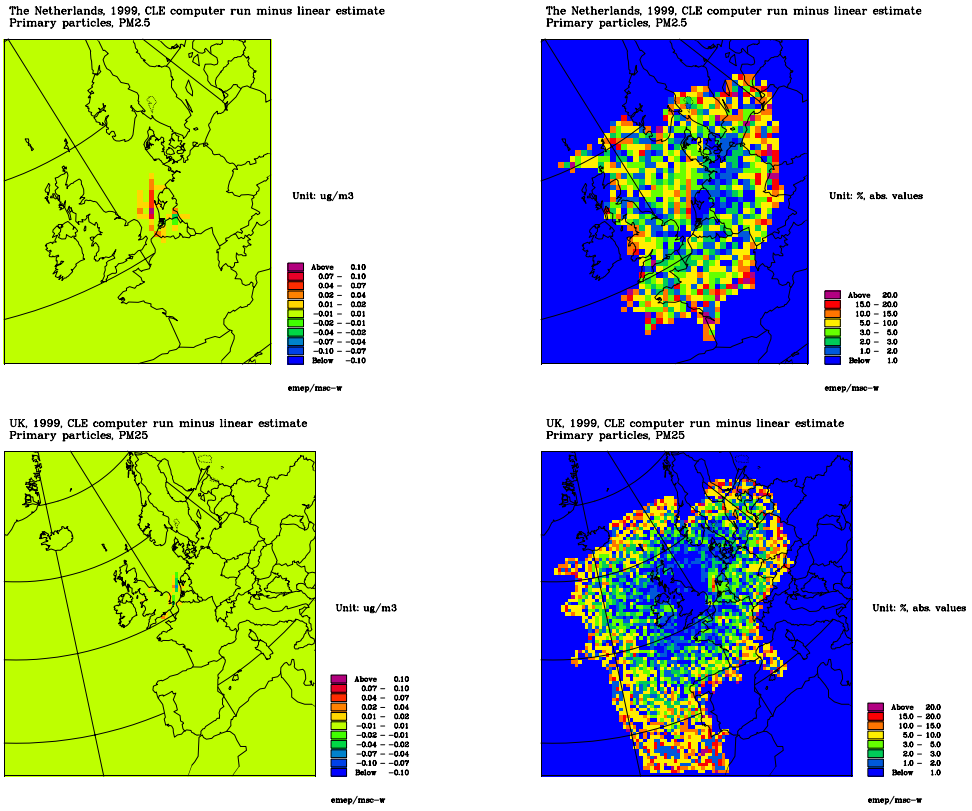

Figure 6.6: Comparison of numerical non-linearities in The Netherlands (above) and in the United Kingdom (below). Figures on the left provide the deviation values from linearity. Figures on the right show non-linear effects as percentage of the primary PM2.5 air concentrations.

on the capability of the Eulerian model to perform source-receptor calculations at European scale.

6.4 Conclusions

In summary, when choosing horizontal and vertical resolution of the Eulerian models one should take into account the physical extension of source regions to make sure that these are sufficiently resolved (more that 2-4 gridcells). Such considerations are particularly important when using Eulerian models for source-receptor applications at national level.

The results show that errors associated with the numerical representation of transport in Eulerian models are small when the physical extension of source regions to be analysed separately is sufficiently resolved. The conclusion is that for European scale applications, when the grouping of cells corresponds to country limits, the Eulerian EMEP model with the present 50x50km^2 resolution can provide country-to-grid source-allocation calculations with reasonable accuracy.

This conclusion is also supported by the results from the NONLIN project for the transport of primary Particulate Matter. According to these calculations, numerical

errors may affect the calculation of source-receptor relationships for small European countries by introducing up to 10-15% differences between model runs and linear calculations. For most European countries, however, the numerical errors in the calculation of country-to-grid are below 3-5%. These results are reassuring on the capability of the Eulerian model to perform source-receptor calculations at European scale.

Further analysis on the effect of non-linearities associated with different chemical processes for nitrogen and ozone and aerosol dynamics processes, will be carried out within the framework of the NONLIN project, in co-operation with CIAM.

6.5 References

Bartnicki, J. , 2000, Non-linear effects in the source receptor matrices computed with the EMEP Eulerian Acid Deposition Model, EMEP/MSC-W Note 4/00, The Norwegian Meteorological Institute, Oslo, Norway.

Berge, E. and Tarrasón, L., 1992, An evaluation of Eulerian advection methods for the modeling on long range transport of air pollution., Norwegian Meteorological Institute, EMEP MSC-W Note 2/92.

Bott, A. , 1989, A positive definite advection scheme obtained by non-linear renormalization of the advection fluxes, *Mon. Weather Rev.*, 117, 1006–1015.

Tsyro, S. and Erdman, L. , 2000, Parameterisation of aerosol deposition processes in emep msc–e and msc–w transport models, MSC-W Note 7/00.

Tsyro, S. and Tarrasón, L. , 2001, Model estimation of particulate matter levels in europe, Technical report, The Norwegian Meteorologial Institute, Oslo,Norway.

Wind, P. , 2002, Development of a modeling system able to link hemispheric- regional and local air pollution problems, MSC-W Note 5/2002.

Chapter 7

Stomatal Ozone Uptake over Europe: Preliminary Results

David Simpson, Mike Ashmore, Lisa Emberson, Juha-Pekka Tuovinen, Margaret MacDougall, Ron I. Smith

7.1 Introduction

This chapter reports briefly on some preliminary results on ozone uptake modelling performed within the EMEP photo-oxidant model. This new version (rv1.2β) contains a deposition module which enables explicit calculation of the stomatal component of surface fluxes. The module has previously been examined and tested mainly in an offline mode, but here we present for the first time calculations made with the module implemented in the full 3-D oxidant model.

This modelling is capable of differentiating between stomatal and non-stomatal ozone flux, and as such enables estimates of the absorbed ozone dose to be made for different vegetation types as a component of total ozone deposition. Stomatal ozone flux (or ozone uptake) is calculated with consideration of vegetation-specific phenology and physiological responses to environmental conditions and as such should improve spatial and temporal assessments of the possible risks of ozone damage to vegetation across Europe.

It should be emphasised that these results are presented for illustration only. Work is still required to improve many of the input databases to the new model, and to deal with soil moisture effects, before proper estimates of ozone uptake can be made. However, the basic features of the ozone uptake modelling are now in place and the results presented here are believed to represent a reasonable first estimate of the spatial and temporal patterns of ozone uptake that exist across Europe.

7.1.1 Background

An Ad-hoc Expert Panel Meeting on "Modelling and Mapping of Ozone Flux and Deposition to Vegetation" was held in Harrogate, UK, between 16-19th June 2002. This meeting was organised to assess the current scientific status of methods to model and map the deposition and flux of ozone to vegetation, in the context of their possi-

ble application in revised critical level assessments for ozone under the review of the Gothenburg Protocol. A main conclusion of the meeting was that there was general agreement that the flux approach represents an improvement on the AOT40 index for the following reasons:

- The existing Level I AOT40 approach is not appropriate for estimates of actual damage and as such should not be used to evaluate economic losses attributable to ozone.
- In contrast, the flux approach, if used in conjunction with appropriate flux-response relationships, could be used to estimate damage and hence economic estimates of ozone impacts.
- There seems to be strong agreement amongst the scientific community regarding the merits of the flux approach for Level II mapping.

7.2 Brief Description of Module

The deposition module has been described and evaluated in a series of publications (Emberson et al, 2000a,2000b,2001, Simpson et al., 2001, Tuovinen et al., 2001). The deposition flux of ozone at a particular height z is calculated as the product of the ozone concentration at height z and the deposition velocity, $V_{g,z}$, at that height. $V_{g,z}$ is calculated using a standard resistance approach, where the resistances used are (1) R_a – aerodynamic resistance between z and the top of the vegetation canopy; (2) R_b – the quasi-laminar layer resistance to ozone transfer; (3) R_c – the surface (canopy) resistance to ozone.

For the regional ozone modelling, we calculate fluxes to a number of land-cover classes within each grid square, using a sub-grid (mosaic) approach, similar to that used previously for the MADE model (Jakobsen et al., 1997, Simpson et al., 2002). Stability and turbulence are first calculated over each landuse, based upon the vegetation characteristics (roughness length, height, LAI). Deposition velocities are then calculated, which can be multiplied by the oxidant model's O_3 concentrations (both estimated at the same reference height) to estimate both total O_3 flux and the stomatal component.

The surface resistance is controlled by various parameters associated with the ground and external leaf surfaces, and by the stomatal conductance of the leaves. It is the stomatal conductance, G_{sto}, which governs the flux of ozone into the leaf itself, and thus controls ozone uptake to the plant. G_{sto} is calculated using a multiplicative model which has been parameterised for a number of different vegetation types:

$$G_{sto} = G_{max}.f_{age}.\max\{f_{min}, f_{light}.f_T.f_{VPD}.f_{SWP}\} \quad (7.1)$$

where G_{max} is the maximum stomatal conductance (m s^{-1}), f_min is the minimum daytime stomatal conductance factor (0–1) and f_x are factors (from 0–1) describing the stomatal conductance relationship with phenology, photon flux density (light), leaf-temperature (T), leaf-to-air vapour-pressure deficit (VPD), and soil-water potential (SWP). For details of the functions used see Emberson et al. (2000b).

It should be noted that this module is used for all depositing gases in the rv1.2β unified model, with stomatal conductances for each gas simply a function of the stomatal

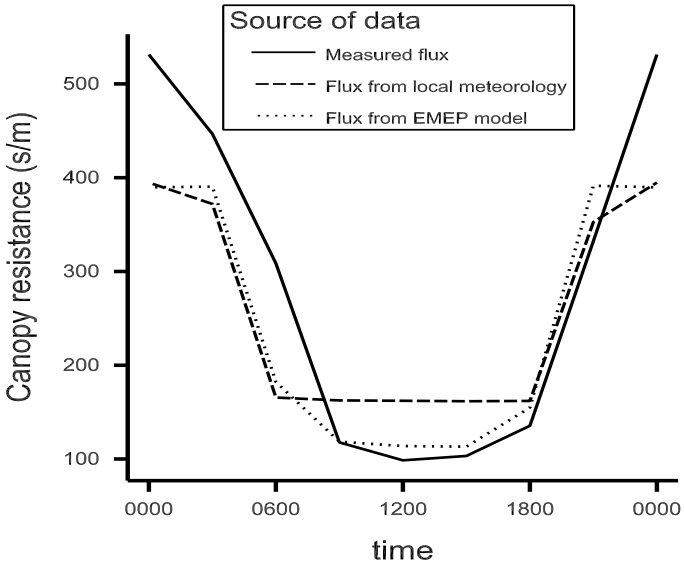

Figure 7.1: Calculated and Observed R_a for Auchecorth Moss (UK), July 1997

conductance for ozone as specified above and the relative molecular diffusivity of the gas relative to ozone. Other conductances are introduced to allow for within-canopy deposition to the ground surface and to the external plant surfaces. These extra terms are often dependant on the solubility of the gas and, in these cases, the conductances are specified for SO_2 and O_3, and interpolated to other gases using reactivity-solubility scaling similar to that suggested by Wesely (1989).

The model structure is sufficiently flexible to include the deposition of gases, such as ammonia, where there is possible emission from the plant canopy alongside deposition, and work to extend the model parameterisation to cover a wider range of gases across Europe is continuing. As part of this process, the deposition model behaviour is being compared to measured flux data from sites in UK, the Netherlands and Germany over a range of vegetation types. In a comparison of ozone fluxes to semi-natural vegetation at Auchencorth Moss (UK), the EMEP model predictions using the 50×50 km^2 meteorology were compared against the deposition calculated from local meteorological observations and against the measured fluxes. There is considerable variability comparing individual observations, as expected, but the overall patterns are encouraging. The hourly median canopy resistances for the month of July 1997 give a diurnal pattern as shown in Figure 7.1. The box-model version of the deposition module used meteorological data from the Norwegian weather prediction model and compares well with the both the measured canopy resistances and those calculated using local meteorology. The high overnight measured canopy resistances are not reflected in output from either model and the canopy resistances from the local meteorology are too high during the period 0900 to 1500. The effect of these discrepancies is being investigated further, but the comparison shows that the EMEP deposition module is achieving a good representation of land use specific canopy resistances.

7.3 Input Data

In order to perform preliminary calculations of ozone flux as presented below, simplified input data have been used. In fact, at the present stage it is probably an advantage to use simple input data in order to better understand the outputs of the ozone uptake modelling. For more realistic estimates of ozone uptake to different vegetation types, these simplified inputs will be replaced by more detailed information.

7.3.1 Land-use, LAI

The land-use data base used in these calculations is based upon that provided by RIVM and used previously in the MADE model. The RIVM database consists of 8 different vegetation classes. Although the intention is to use a much more detailed land-use database from the Stockholm Environment Institute (SEI) in future, time precluded using this for the present study.

However, the following assumptions have been made in an attempt to mimic the SEI land-use classes and their characteristics as given in Emberson et al. (2000b). The RIVM classes do not distinguish between temperate and Mediterranean vegetation, and have a broad "other" vegetation category. For this preliminary study we have assumed that vegetation (forest, crops) north of 45°N is temperate, and south of 45°N is Mediterranean. North of 60°N we assume that RIVM's "other" category is "Tundra", south of 45°N we assume Mediterranean scrub, otherwise "moorland".

Leaf area index (LAI) is a key parameter in deposition modelling. Values of LAI are currently specified for each vegetation type as detailed in Emberson et al. (2000b). The one exception is that for forests we have reduced LAI (and forest height) by 50% north of 62°, in order to generate more realistic values for Nordic conditions (e.g. Tuovinen et al., 2001).

7.3.2 Growing Seasons

Growing seasons for the different vegetation types are currently based upon the default parameterisations given in Emberson et al. (2000b). For crops a latitude-based growing season is used. In the Mediterranean the growing season starts around mid-March, whereas at 60°N it doesn't start until mid-May. This difference in growing season has important implications for the modelling of ozone fluxes.

7.4 Calculations

Here we present preliminary calculations from the EMEP model rv1.2β for the year 1999. It should be noted that soil moisture deficits have not been included in the current modelling scheme, this may generate significant overestimations of stomatal flux for some vegetation types, especially in southern Europe. However, the use of this algorithm for irrigated crops in such regions would be expected to provide realistic predictions of stomatal flux.

It should be noted that the calculations are given as nmol O_3 m^{-2} s^{-1} on a ground area basis. The data given in each figure do not represent the actual coverage of a particular vegetation type, but just the presence of such vegetation within the 50×50

km^2 EMEP grid. (Where a vegetation category is not present in the RIVM data base for a particular area, no results are shown).

7.5 Results

Figure 7.2 illustrates the monthly stomatal uptake of ozone for grasslands over Europe, from March to August. Grasslands were chosen for this first example, since they are present all year round and cover large areas of Europe. The seasonal variation in ozone uptake is apparent, with low ozone uptake values predicted for March followed by progressive monthly increases in ozone uptake to July from when values start to decrease again in August. An important feature of the months when ozone uptake is relatively high is that the fields of calculated uptake are rather uniform. For example, in June ozone uptake values range between 4-6 nmol O_3 m^{-2} s^{-1} over nearly the whole of Europe. (It should be noted though that the incorporation of the soil water deficit component of the modelling algorithm might reduce this uniformity somewhat, as uptake values in the Mediterranean region would be lower.)

Figure 7.3 illustrates the monthly stomatal uptake of ozone for crops, again from March to August. The strongest feature now is the marked seasonal variation. As mentioned in section 7.3.2 the growing seasons of crops are determined using a latitudinal model. Thus, the growing season starts in March in the Mediterranean, and not until May for Scandinavian countries. Further, for crops this season is assumed to last 3 months, so that in effect a band of growth moves northwards as the year progresses. This movement is clearly reflected in the uptake patterns in Figure 7.3.

7.6 AOT40

Figure 7.4 shows the AOT40 values predicted by the model for both crops and forests. Values are clearly highest in the Mediterranean areas, and very strong gradients exist between this area and the rest of Europe. These spatial patterns are clearly different from the O_3 uptake patterns for grasslands and crops presented above.

7.7 Conclusions

First, the caveats of this study need to be stated. The results are very preliminary, not least because the revised EMEP model is still very new and the deposition module just implemented. Many inputs are provisional, notably the leaf area index values, and growing season calculation. More work is needed to estimate soil moisture deficit. Clearly further analysis of the model outputs are required, and further evaluation of the model should also be performed, especially for areas in southern Europe where the reduction in stomatal conductance due to low humidities and soil moisture is a regular occurrence.

Despite these caveats, the results presented above do allow a number of important conclusions to be made. It seems clear that patterns of ozone uptake and patterns of AOT40 can be very different. Further, ozone uptake rates seem to have a much more uniform distribution across Europe than AOT40. Similar results were found in an earlier study, based upon the Lagrangian model, of Emberson et al. (2000a). The

difference between AOT40 and uptake is largely due to the fact that in central and southern Europe, the meteorological conditions which favour ozone formation (high temperatures, and hence high vapour-pressure deficits) tend to inhibit stomatal conductance and hence uptake. Thus elevated ozone can contribute to the AOT40 index but not to uptake. In northern Europe, on the other hand, the cooler, more humid conditions, tend to promote stomatal conductance under typical conditions causing even moderate ozone concentrations to result in significant levels of ozone uptake to the plant. As such, concentrations of ozone below 40 ppb (common in northern areas), which are discounted entirely in the AOT40 index, may contribute to ozone uptake rates.

7.8 References

Emberson, L. , Ashmore, M.R. , Cambridge, H.M. , Simpson, D. , and Tuovinen, J.P. , 2000a, Modelling stomatal ozone flux across Europe, *Environmental Pollution*, 109, No. 3, 403–414.

Emberson, L. , Simpson, D. , Tuovinen, J.-P. , Ashmore, M.R. , and Cambridge, H.M. , 2000b, Towards a model of ozone deposition and stomatal uptake over Europe, EMEP MSC-W Note 6/2000.

Emberson, L.D. , Ashmore, M.R. , Simpson, D. , Tuovinen, J.-P. , and Cambridge, H.M. , 2001, Modelling and mapping ozone deposition in Europe, *Water, Air and Soil Pollution*, 130, 577–582.

Jakobsen, H. A. , Jonson, J. E. , and Berge, E. , 1997, The multi-layer Eulerian model: Model description and evaluation of transboundary fluxes of sulphur and nitrogen for one year, EMEP/MSC-W Report 2/97, The Norwegian Meteorological Institute, Oslo, Norway.

Simpson, D. , Tuovinen, J.-P. , Emberson, L.D. , and Ashmore, M.R. , 2001, Characteristics of an ozone deposition module, *Water, Air and Soil Pollution: Focus*, 1, 253–262.

Simpson, D. , Tuovinen, J.-P. , Emberson, L.D. , and Ashmore, M.R. , 2002, Characteristics of an ozone deposition module, *Water, Air and Soil Pollution*, To be published.

Tuovinen, J.-P. , Simpson, D. , Mikkelsen, T.N. , Emberson, L.D. , M., M. R. Ashmore , Aurela, Cambridge, H. M. , Hovmand, M. F. , Jensen, N. O. , Laurila, T. , Pilegaard, K. , and Ro-Poulsen, H. , 2001, Comparisons of measured and modelled ozone deposition to forests in Northern Europe, *Water, Air and Soil Pollution: Focus*, 1, 263–274.

Wesely, M.L. , 1989, Parameterization of surface resistances to gaseous dry deposition in regional scale numerical models, *Atmospheric Environment*, 23, 1293–1304.

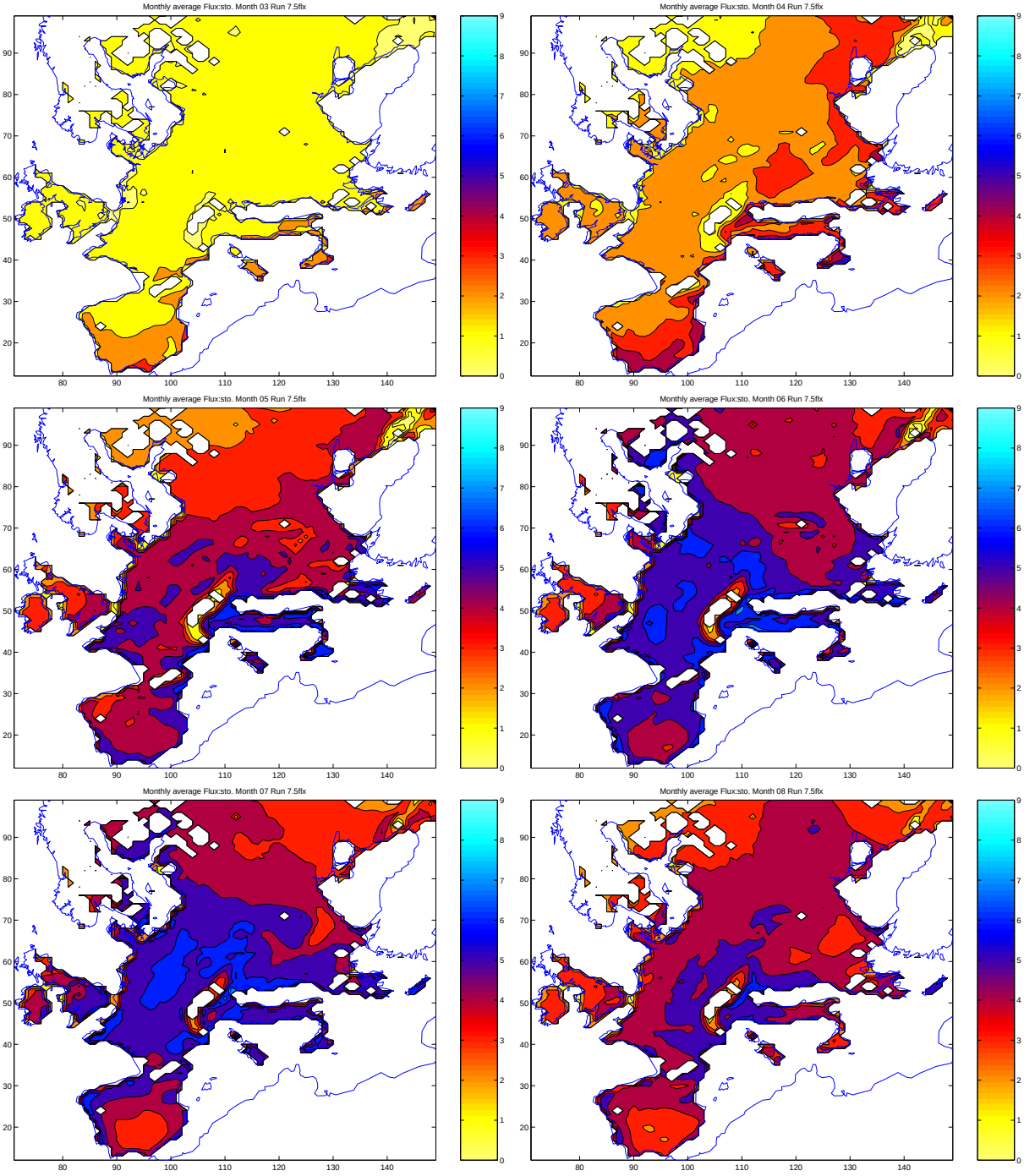

Figure 7.2: Estimated stomatal fluxes to grasslands, March (top left) to August (bottom right). Units: nmol m^{-2} s^{-1}. Estimates are only available where the landuse data-base shows grasslands, otherwise area is blank.

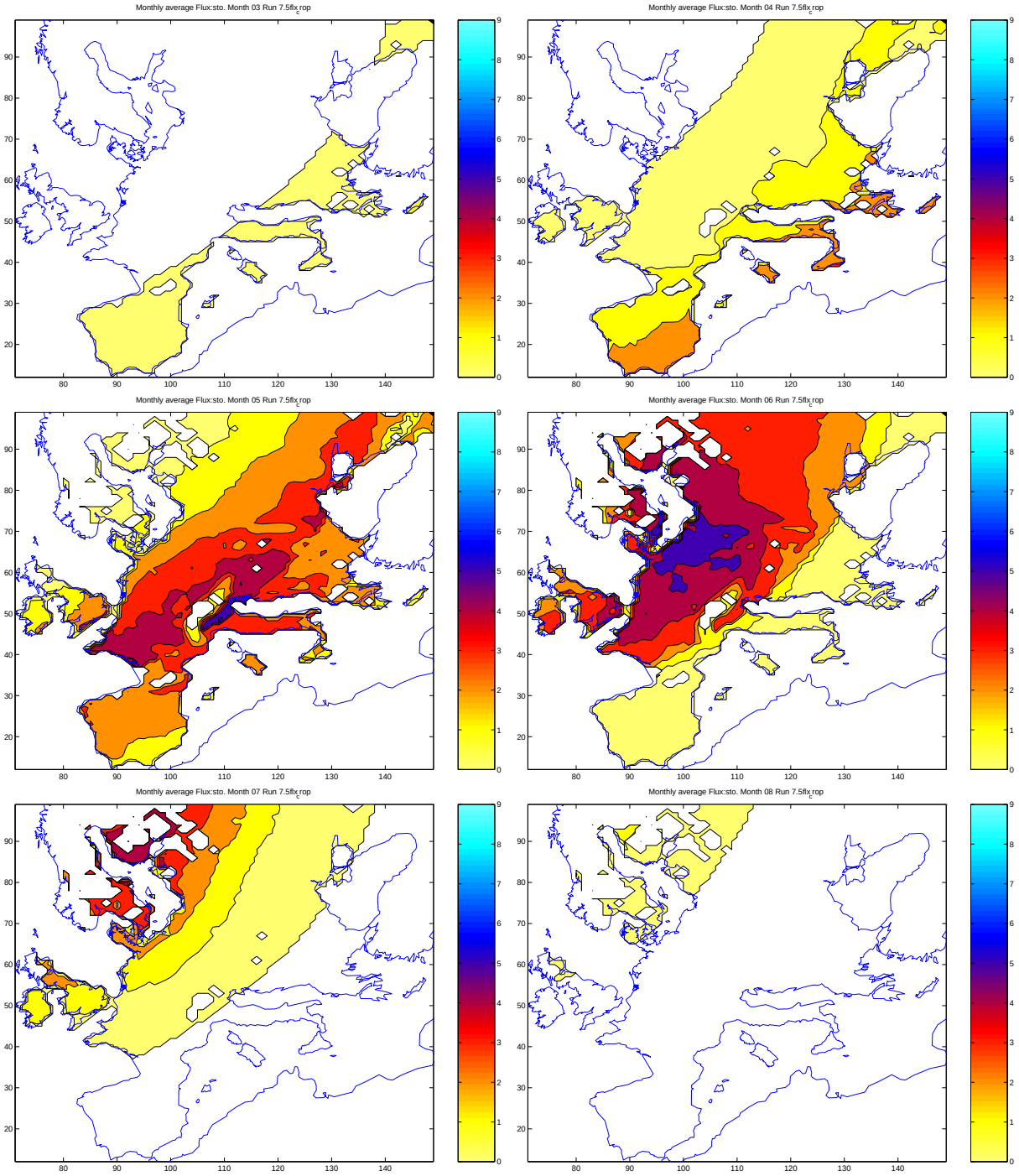

Figure 7.3: Estimated Stomatal fluxes to crops, March (top left) to August (bottom right). Units: nmol m^{-2} s^{-1}. Estimates are only available where the landuse data-base shows crops, otherwise area is blank.

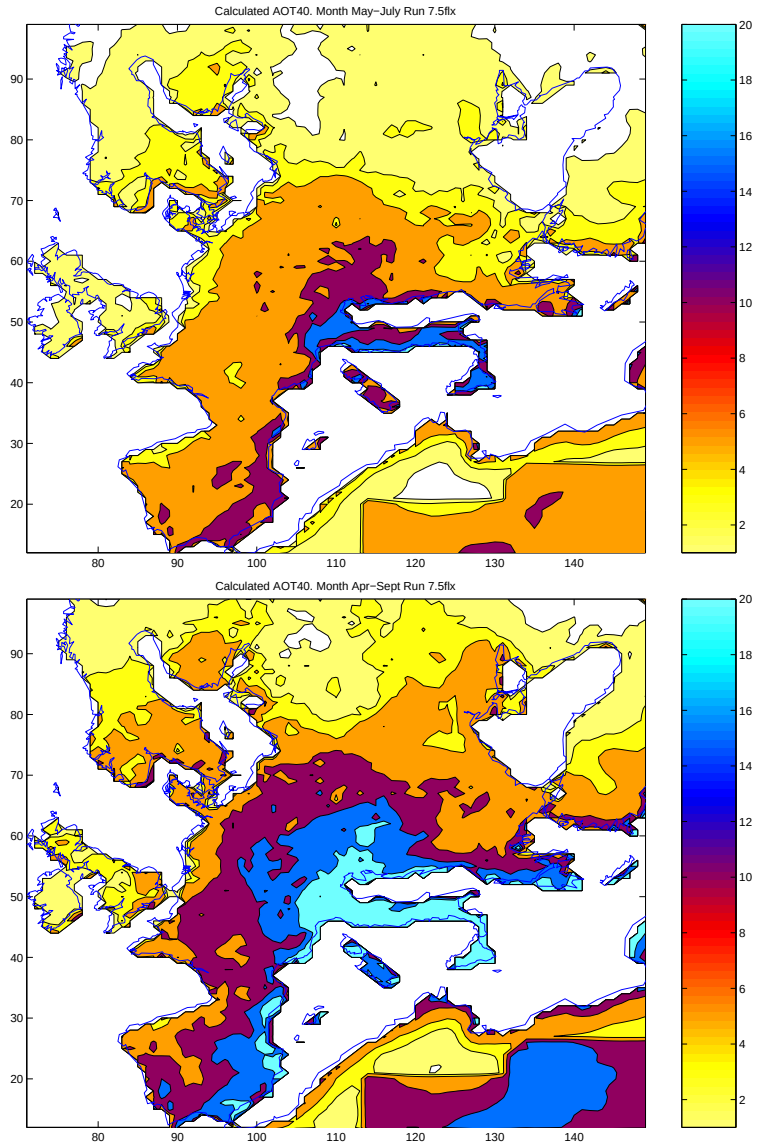

Figure 7.4: Calculated AOT40 for Crops (top) and Forests (bottom), from EMEP model (rv1.2β) calculations for 1999. Units: ppm.h

Chapter 8

Conclusions and Outlook

Some of the main conclusions to be drawn from this report are:

- The EMEP MSC-W Eulerian model system has undergone a substantial overhaul. Several previous EMEP models (Lagrangian as well as Eulerian) has been merged and re-written in order to produce a single core model system. The new system implements the older acid-deposition, ozone, and aerosol models as sub-versions of the core model.

- A basic version of the model is up and running, and produces results which are generally comparable, if not better, than results from previous EMEP models.

- Annual average of NO_2 concentrations for EMEP stations are in general within a factor of 2, and timeseries of NO_2 show the expected seasonal trends. Calculated concentrations of SO_2 and SO_4^{2-} correlate well with observations, both in timeseries and as annual averages, but SO_2 is somewhat overestimated. Concentrations in precipitation of sum of nitrate, total sulphate and ammonia plus ammonium agree very well with observations, and for most stations the model data are within the '30% limit'.

- Seasonal and daily variations in species such as ozone are reproduced well. The comparison with ozone-sonde observations show that the model overestimates ozone in the middle to upper free troposphere. The effect of this overestimation on surface ozone is likely to be limited. It is encouraging to see that for ozone and formaldehyde model results are improved with the rv1.2β version of the model.

- Investigations show that numerical errors associated with the representation of transport in the Eulerian model are small when the physical extension of source regions to be analysed separately are sufficiently resolved. The conclusion is that for European scale applications, the Eulerian EMEP model can provide country-to-grid source-allocation calculations with reasonable accuracy.

- A number of weak areas have been identified, for example the need for a better description of SO_2 to sulphate oxidation, and verification of important boundary layer parameters. These subjects will be investigated and hopefully result in an improved version of the model within the near future.

- For the first time, we have been able to show model results for the stomatal uptake of ozone into vegetation across Europe. The requirements of the critical-levels community for oxidant models which can predict stomatal fluxes as well as concentrations are well on the way to being met. Preliminary results suggest that patterns of stomatal uptake are rather different to those of AOT40. A major task is now to evaluate these model predictions against measurements of ozone concentrations and deposition across Europe.

The implementation of an aerosol dynamics model has also been accomplished within the unified model system. This work is reported in an accompanying EMEP Note Tsyro (2002).

As noted last year, the measurements of carbonyls and hydrocarbons available within EMEP have proven extremely valuable in evaluating both the models and the emission inventories. It is recommended that such measurements continue and if possible be enhanced with other key-species for evaluating photochemical models, for example NO_y constituents and radical concentrations. With a new focus on stomatal flux modelling, additional measurements of the deposition of ozone and/or other gases at some stations would be invaluable for building confidence in such modelling, and in evaluating trends in ozone uptake.

References

Tsyro, S. , 2002, First estimates of the effect of aerosol dynamics in the calculation of PM10 and PM2.5, MSC-W Note 4/2002.